LBL--16892

DE84 004351

THE AUGER DECAY MECHANISM IN PHOTON-STIMULATED DESORPTION OF IONS FROM SURFACES

Christopher Carr Parks
(Ph.D. Thesis)

Materials and Molecular Research Division
Lawrence Berkeley Laboratory

and

Department of Chemistry
University of California
Berkeley, California 94720

November 1983

DISCLAIMER

This report was prepared as an account of work sponsored by an agency of the United States Government. Neither the United States Government nor any agency thereof, nor any of their employees, makes any warranty, express or implied, or assumes any legal liability or responsibility for the accuracy, completeness, or usefulness of any information, apparatus, product, or process disclosed, or represents that its use would not infringe privately owned rights. Reference herein to any specific commercial product, process, or service by trade name, trademark, manufacturer, or otherwise does not necessarily constitute or imply its endorsement, recommendation, or favoring by the United States Government or any agency thereof. The views and opinions of authors expressed herein do not necessarily state or reflect those of the United States Government or any agency thereof.

This work was supported by the Director, Office of Energy Research, Office of Basic Energy Sciences, Chemical Sciences Division of the U.S. Department of Energy under Contract No. DE-AC03-76SF00098. It was performed at the Stanford Synchrotron Radiation Laboratory, which is supported by the Department of Energy, Office of Basic Energy Sciences and the National Science Foundation, Division of Materials Research.

MASTER

THE AUGER DECAY MECHANISM IN
PHOTON-STIMULATED DESORPTION OF IONS FROM SURFACES

Contents

THE AUGER DECAY MECHANISM IN PHOTON-STIMULATED DESORPTION OF IONS FROM SURFACES

Christopher Carr Parks

Materials and Molecular Research Division
Lawrence Berkeley Laboratory
and
Department of Chemistry
University of California
Berkeley, California 94720

ABSTRACT

Photon-stimulated desorption (PSD) of positive ions was studied with synchrotron radiation using an angle-integrating time-of-flight mass spectrometer. Ion yields as functions of photon energy near core levels were measured from condensed gases, alkali fluorides, and other alkali and alkaline earth halides. These results are compared to bulk photoabsorption measurements with emphasis on understanding fundamental desorption mechanisms. The applicability of the Auger decay mechanism, in which ion desorption is strictly proportional to surface absorption, is discussed in detail. The Auger decay model is developed in detail to describe Na^+ and F^+ desorption from NaF following Na(1s) excitation. The major decay pathways of the Na(1s) hole leading to desorption are described and equations for the energetics of ion desorption are developed. Ion desorption spectra of H^+, Li^+, and

F^+ are compared to bulk photoabsorption near the F(2s) and Li(1s) edges of LiF. A strong photon beam exposure dependence of ion yields from alkali fluorides is revealed, which may indicate the predominance of metal ion desorption from defect sites. The large role of indirect mechanisms in ion desorption from condensed N_2-O_2 multilayers is demonstrated and discussed. Ion desorption spectra from several alkali halides and alkaline earth halides are compared to bulk photoabsorption spectra. Relative ion yields from BaF_2 and a series of alkali halides are discussed in terms of desorption mechanisms.

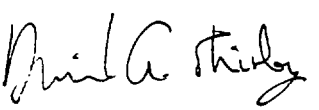

I. INTRODUCTION

In this Introduction, current topics in photon-stimulated desorption research are presented in Part A, while the organization of the thesis is described in Part B.

A. Topics in Photon-Stimulated Desorption Research

Since the discovery of electron-stimulated desorption (ESD) thresholds at core level binding energies[1,2] and the discovery[3] of photon-stimulated desorption (PSD) of positive ions in 1979, interest in stimulated desorption as a surface probe has increased enormously. In PSD, photons impinge on a surface and, by means of an electronic transition, cause ions to desorb from the surface. In the Auger decay model of Knotek and Feibelman,[1,2] the initial step of desorption is ionization of a core level, followed by an Auger decay cascade and production of a multihole final state. A surface anion species becomes positively charged and may be expelled from the surface. While originally proposed to explain anion species desorbing as positive ions from metal oxides, the Auger decay model has been extended to encompass desorption from many materials.[4] Developments in the description of the Auger decay model are presented in Chapter III.

PSD is a local, site-specific probe in the Auger decay model. Ion yields are directly proportional to photoabsorption of surface sites participating in the desorption. When the Auger decay mechanism

predominates, PSD can be used as a probe of absorption of surface sites: ion yield spectra as functions of photon energy show near edge and extended x-ray absorption fine structure (EXAFS). An EXAFS analysis can give nearest-neighbor bond distances. In PSD EXAFS, the nearest-neighbor distances in particular bonding sites could be determined.

In a general view of desorption,[5] a transition occurs within the Franck-Condon approximation to a repulsive excited state followed by desorption in competition with delocalization of the excitation. This general framework is codified[6,7] in desorption literature as the Menzel-Gomer-Redhead (MGR) model. The Auger decay model is included in this general framework as an important special case. Of course, a true MGR calculation is intractable for any real surface. In the past, analysis was limited to using generic Franck-Condon diagrams to predict trends. Only recently have experimental results been interpreted successfully using cluster calculations of ground and excited states: Melius, Noell, and Stulen[8] described the double excitations responsible for H^+ desorption from Ni(111) following valence level excitation. The Auger decay mechanism fails in O^+ desorption from CO/Ni(100) above the O(K) edge, and bond breaking occurs via multielectron excitations.[9]

When the general MGR model needs to be invoked, the strict proportionality of PSD to surface absorption is lost; this strict proportionality of the Auger decay mechanism generated the excitement about PSD as a surface science technique in 1979. For the surface

scientist wishing to extract information about a variety of surfaces, failures of the Auger decay mechanism are unwelcome; for the theoretically-minded, the need to use the MGR mechanism is seen as a challenge.

Jaeger et al. demonstrated[10] that x-ray induced ESD, in which secondary electrons travel through the lattice and desorb ions from the surface, is a major mechanism in desorbing H^+ from NH_3 multilayers. Indirect mechanisms such as X-ray induced ESD destroy the site-specific nature of PSD, making the technique of minimal value as a surface probe. Cases in which indirect mechanisms prevail are unwelcome to both the surface scientist and the MGR-mechanism theoretician; only the materials scientist interested in secondary damage processes has modest interest. New data on indirect mecnanisms in PSD are described in detail in Chapter V.

Desorption yields are displayed in Table I. Measures of desorption yield efficiences are ions per photon or, more fundamentally, ions per surface ionization. Ion yields are very high following K-shell ionization of van der Waals solids,[11] in which substantial x-ray induced ESD may occur and in which energy is localized in the molecular subunits following Auger decay. For valence excitation of condensed gas multilayers[11] and for O(K) shell excitation of CO/Ni(100),[9] in which desorption does not occur by the Auger decay mechanism, ion yields are lower. H^+ yields from nd and 4f metal oxides are high,[12,13] and are very sensitive to valency.[1,2] Yields from alkali halides are low and have unusual

beam exposure properties. By contrast, excited Li in the $^2P^0$ state desorbs with high intensity[14] from LiF.

These small ion desorption efficiencies are the consequence of basic physics. Ion desorption, by any of the standard mechanisms, occurs in several steps:

1. The photoabsorption event (10^{-16} s).
2. The fast (10^{-15} s) electronic distribution of energy.
3. The slow (10^{-12} s) ejection of the ion having several electron volts kinetic energy.

The crucial feature is the direct coupling of slow desorption to electronic excitations. Because of energy dissipation into the solid, most surface ionizations do not result in desorption. Much theoretical effort concerns the nature of the long-lived multihole states necessary for desorption to occur. In the approach initiated by Cini and Sawatzky,[15,16] when the hole-hole correlation energy greatly exceeds the valence band width, hole-hole diffusion times can be long, allowing desorption to take place.[17,18]

These modest ion yields impose practical limitations and fundamental questions. With photon fluxes available today at synchrotron radiation sources, PSD EXAFS studies are intensity limited, and only a few experiments have been accomplished.[12] A vital question is whether PSD occurs weakly but homogeneously on a sample, or whether it occurs from special minority sites. Currently, in adsorbate systems, answers are determined on a case-by-case basis, by careful measurements of ion yield versus adsorbate exposure. In

Chapter IV, dependences of Na^+ and H^+ yields from NaF on photon beam exposures are described. These results indicate that defect properties may predominate in ion desorption from alkali halides. Time or photon-beam dependences of H^+ yield from freshly cleaved Si(111) surfaces also occur.[19] In these cases, stimulated desorption is a poor probe of majority sites. On the other hand, if the PSD-active defect sites prove to be interesting in their own right, PSD would have unique capabilities.

In summary, PSD is a recently-discovered and complex process which holds promise as a surface probe. In 1979, excitement was generated by the discovery of ion desorption thresholds at core edges and the formulation of the Auger-decay model of desorption. Using the strict proportionality of ion yield and photoabsorption of surface sites inherent in the Auger decay model, one can obtain detailed electronic and structural information about specific surface sites using near-edge fine structure and EXAFS. Since 1979, desorption thresholds at core edges of many materials were found, which were interpreted as evidence for the Auger decay mechanism. However, the dominance of x-ray induced electron stimulated desorption (XESD), in which secondary electrons desorb ions, was demonstrated in ammonia multilayers. Some of the observations of ion desorption thresholds at core edges could also be explained by XESD. A major role of the more general Menzel-Gomer-Redhead model was demonstrated in both valence and core-level excitation of certain systems. Desorption from minority surface sites predominates from some insulator,

semiconductor, and adsorbate materials. Therefore, PSD is very complex, and fundamental questions must be answered before PSD can become a standard surface probe.

B. Organization of the Thesis

Currently, PSD is most useful as a surface science technique when the Auger decay model predominates. Therefore, much of this thesis is devoted to developing the Auger decay model and determining its limitations. The thesis is organized as follows:

In the experimental section of Chapter II, properties of the PSD time-of-flight detector are described and recent absolute flux measurements of beam line III-1 at the Stanford Synchrotron Radiation Laboratory are documented.

In Chapter III, the Auger decay mechanism is described in detail for desorption from sodium fluoride following Na(1s) excitation. The Auger decay mechanism is extended to include desorption of Na^+ as well as F^+ ions. Expressions for the maximal energies available to the desorbing Na^+ and F^+ ions are derived. Support for the Auger decay mechanism is found in the agreement of ion yield and absorption spectra.

In Chapter IV, ion desorption from LiF near the Li(1s) and F(2s) edges is studied and photon beam dependences of ion yields from LiF and NaF are described. In the Auger decay model, one might expect desorption thresholds of both F^+ and Li^+ at the F(2s) and Li(1s) edges. In fact, only F^+ has a threshold at the F(2s) edge.

Therefore, F^+ may desorb in an Auger decay process, while the origin of Li^+ desorption is uncertain. Metal and hydrogen ion yields are strongly affected by beam exposures which could only act directly on a minute fraction (10^{-5}) of a monolayer. These results demonstrate the importance of defect properties in ion desorption from alkali halides.

In Chapter V, it is shown that a strong indirect mechanism contributes to N^+ desorption from a N_2-O_2 solid mixture at the O(K) edge. The role of x-ray induced electron stimulated desorption as an indirect desorption mechanism is examined in terms of molecular electron and photon absorption cross sections. The implications concerning the surface sensitivity of PSD and ESD in general are discussed.

In Chapter VI, results of PSD measurements from several alkali halides and alkaline earth halides are reported. Ion desorption spectra from KF, CaF_2, and BaF_2 were found to resemble bulk photoabsorption at various edges, in agreement with the Auger decay mechanism of desorption. Ion desorption of F^+ and Ba^{2+} is shown to be exothermic, but no Ba^{2+} yield was obtained in experiment. Ion yields from a series of alkali halides exhibit large variations in yield which cannot be explained by photoabsorption cross sections or by a model of hole-hole lifetimes.

Chapter VII provides a historical perspective of significant developments as well as some thoughts on the future of the PSD technique.

TABLE I. Photon-stimulated desorption yields from selected materials

SYSTEM	DESORBED SPECIES	LEVEL EXCITED	YIELD PER PHOTON[a]	YIELD[b] PER SURFACE IONIZ	REFERENCE[c]
N_2 solid	N^+	N(1s)	4×10^{-6}	10^{-3}	Ref. 11
CO/Ni(100)	O^+	O(1s)	2×10^{-7}	10^{-4}	Ref. 9
N_2 solid	N^+	Valence	2×10^{-8}	10^{-6}	Ref. 11
C_2H_2 solid	H^+	Valence	4×10^{-7}	10^{-5}	Ref. 11
Mo(100)/O	O^+	Mo(2s)	1×10^{-5}	10^{-2}	Ref. 12
Si(111)/H	H^+	Si(K)	8×10^{-10}	10^{-5}	Ref. 19
NaF (100)	Na^+	Na(1s)	6×10^{-9}	10^{-5}	Chap. III
LiF	Li $^2P^0$	Li(1s)	7×10^{-3}	------	Ref. 14

a Assuming, for consistency with the literature, unity detection efficiency. Based on microchannel plate efficiencies to ions, an upper bound on detector efficiency is 20 percent. The PSD cross section is the yield per photon divided by the surface coverage of about 10^{15} cm^2.

b The number (I) of surface ionizations per second was estimated using $I = \sigma(h\nu)\ F(\text{photons/sec})\ \rho(cm^{-2})$, where σ is the photoabsorption coefficient, F is the photon flux, and ρ is the surface coverage ($10^{15}/cm^2$). Atomic and molecular photoabsorption cross sections were used in these rough estimates. In order in Mb units, these were 2.3(Ref. 20), 0.4(Ref. 21), 15(Ref. 22), 13(Ref. 22), 0.32(Ref. 23), 0.12(Ref. 23), 0.2(Ref. 24,25), and ---.

c For references in which I (CCP) am a co-author, ion yields were estimated from the original data and do not always appear in the reference.

REFERENCES

1. M. L. Knotek and P. J. Feibelman, Phys. Rev. Lett. 40, 964 (1978).

2. P. J. Feibelman and M. L. Knotek, Phys. Rev. B 18, 6531 (1978).

3. M. L. Knotek, V. O. Jones, and V. Rehn, Phys. Rev. Lett. 43, 300 (1979).

4. For a general review of all aspects of ion desorption: Proceedings of the First International Workshop on Desorption Induced by Electronic Transitions (DIET-1), (Williamsburg, Virginia, 1982), edited by N. H. Tolk, M. M. Traum, J. C. Tully, and T. E. Madey (Springer-Verlag, Berlin, 1983).

5. D. Menzel in Proceedings of the First International Workshop on Desorption Induced by Electronic Transitions (DIET-1), (Williamsburg, Virginia, 1982), edited by N. H. Tolk, M. M. Traum, J. C. Tully, and T. E. Madey (Springer-Verlag, Berlin, 1983), page 53.

6. P. A. Redhead, Can. J. Phys. 42, 886 (1964).

7. D. Menzel and R. Gomer, J. Chem. Phys. 41, 3311 (1964).

8. C. F. Melius, J. O. Noell, and R. H. Stulen, J. Vac. Sci. Technol. 20, 559 (1982).

9. R. Jaeger, J. Stöhr, R. Treichler, and K. Baberschke, Phys. Rev. Lett. 47, 1300 (1981).

10. R. Jaeger, J. Stöhr, and T. Kendelewicz, Phys. Rev. B 28, 1145 (1983).

11. R. A. Rosenberg, V. Rehn, A. K. Green, P. R. LaRoe, and C. C. Parks in Proceedings of the First International Workshop on

Desorption Induced by Electronic Transitions (DIET-1), (Williamsburg, Virginia, 1982), edited by N. H. Tolk, M. M. Traum, J. C. Tully, and T. E. Madey (Springer-Verlag, Berlin, 1983), page 247.

12. R. Jaeger, J. Stöhr, J. Feldhaus, S. Brennan, and D. Menzel, Phys. Rev. B 23, 2102 (1981).
13. B. E. Koel, G. M. Loubriel, M. L. Knotek, R. H. Stulen, R. A. Rosenberg, and C. C. Parks, Phys. Rev. B 25, 5551 (1982).
14. N. H. Tolk, M. M. Traum, J. S. Kraus, T. R. Pian, W. E. Collins, N. G. Stoffel, and G. Margaritondo, Phys. Rev. Lett. 49, 812 (1982).
15. G. A. Sawatzky, Phys. Rev. Lett. 39, 504 (1977).
16. M. Cini, Solid State Commun. 24, 681 (1977).
17. D. E. Ramaker, C. T. White, and J. S. Murday, Phys. Lett. 89A, 211 (1982).
18. P. J. Feibelman, Surf. Sci. 102 L51 (1981).
19. M. L. Knotek, G. M. Loubriel, R. H. Stulen, C. C. Parks, B. E. Koel, and Z. Hussain, Phys. Rev. B 26, 2292 (1982).
20. H. Petersen, A. Bianconi, F. C. Brown, and R. Z. Bachrach, Chem. Phys. Lett. 58, 263 (1978).
21. S. M. Goldberg, C. S. Fadley, and S. Kono, J. Elect. Spec. and Relat. Phenom. 21, 285 (1981).
22. J. Berkowitz, Photoabsorption, Photoionization, and Photoelectron Spectroscopy, (Academic Press, New York, 1979).
23. B. L. Henke, P. Lee, T. J. Tanaka, R. L. Shimabukuro, and B. K.

Fujikawa, At. Data and Nucl. Data Tables 27, 1 (1982).

24. I. M. Band, Yu. I. Kharitonov, and M. B. Trzhaskovskaya, At. Data Nucl. Data Tables 23, 443 (1979).

25. G. V. Marr and J. B. West, At. Data Nucl. Data Tables 18, 497 (1976).

II. EXPERIMENTAL

Each chapter is a fully contained unit, with experimental details pertinent to the given chapter. Here, I shall concentrate on aspects which are not discussed elsewhere. I shall briefly discuss the data system and the three experimental chambers in Part A. In Part B, I shall describe the properties of the time-of-flight mass spectrometer in detail. In Part C, the photon flux of one of the photon beam lines used extensively in this thesis shall be documented.

A. General Description of Apparatus

In these measurements, three separate chambers were used for different experiments, which I will call the Sandia, the China Lake, and the VG chamber. All chambers contained the usual surface science equipment, a channeltron for total electron yield measurements, and a PSD detector. The Sandia chamber was equipped with a sample cleaver and sample transfer system, so that many cleavable crystals could be used witnout breaking vacuum. The China Lake chamber had a special manipulator with a liquid helium cryostat for condensed gas studies. Thick condensed multilayers were grown on the Al_2O_3 substrate at temperatures between 10-30 K. These temperatures were sufficient to grow films such as N_2 while keeping the chamber in the 10^{-10} torr range. The Vacuum Generators (VG) chamber was equipped with an electron energy analyzer (VG model ADES-400).

The experimental layout is shown in Fig. 1. Synchrotron radiation emerging in pulses from the storage ring was monochromatized

and passed through a beam flux monitor (labeled "I_0 Signal") before striking the sample. Ions desorbed from the sample, were accelerated into the PSD detector, and were detected by microchannel plates. The microchannel plate signal was amplified, discriminated, and fed into the START of a time to amplitude converter (TAC). A 1.28 Mhz clock provided the signal for the STOP input. Because the ion species arrived at different times, the TAC output provided a different amplitude pulse for each ion species. The TAC output was fed into a multichannel analyzer (MCA), which accumulated and displayed the time-of-flight mass spectrum. Because the timing resolution required (1-3 ns) was not stringent, commercial timing electronics were used. The data were stored in an LSI-11 (or, for the China Lake experiments, a HP-9825) minicomputer.

To measure the photon flux, electron yield from the metal grid was collected onto a positively-biased channeltron. The channeltron amplified the signal, which passed through a high voltage battery box to a picoammeter. The picoammeter output was converted for digital storage using a voltage to frequency converter and a scaler.

The minicomputer collected all data and controlled the monochromator energy. The areas of the ion mass peaks were integrated, normalized to the photon flux, and plotted. The data were stored on floppy disks for easy access later. When the experiment was proceeding smoothly, it was possible for one relaxed scientist to preside. However, unforeseen events were known to occur.

B. The Time-of-Flight Mass Spectrometer

Characteristics of the time-of-flight mass spectrometer used in the PSD measurements are considered in this section. The time-of-flight technique is optimal for synchrotron radiation studies if the mass resolution requirements are modest. The detector geometry, operating voltages, and estimated overall efficiency are documented. I treat the ion trajectory problem, and show that kinetic energy and angle distributions of desorbing ions can be obtained from an angle-resolving time-of-flight spectrometer, but only with much more effort. An experimental time-of-flight mass spectrum is compared to the results of a simple trajectory calculation.

The PSD time-of-flight analyzer of Fig. 2 consists of a grid to accelerate ions from the grounded sample, a drift tube, two microchannel plates to detect and amplify the signal, and a collector. A synchrotron radiation pulse arrives at the sample every 780 ns causing positive ions to desorb. The ions, having initial kinetic energies of 0-10 eV, are accelerated into the drift tube, and hit the microchannel plates. The typical distance between the sample and the drift tube is 1.5 cm and the drift tube length is 5.7 cm. The drift tube voltage is between -500 and -1800 V and the front face of the first microchannel plate is between -1900 and -2000 V. With these distances and voltages times-of-flight of masses 1-20 amu are between 0 and 1000 ns. The collection efficiency is very high because the analyzer is angle integrating. The detection efficiency is limited by the microchannel plates[1] to about 25 percent for 2000 eV ions. The microchannel

plate efficiency as a function of mass[2,3] may vary by 30 percent. Therefore, an nominal upper bound on overall analyzer detector efficiency is 20-30 percent.

Electrostatic time-of-flight analyzers have useful general characteristics. For any one dimensional force along x depending on position only, the time t as a function of position can be written

$$t-t_0 = m^{1/2} \int_{x_0}^{x} \frac{dx}{[2(U_0 + qV_0 - qV(x))]^{1/2}} , \qquad (1)$$

where m is the mass, U_0 the initial kinetic energy, q the charge, V(x) the potential, and V_0 the potential at the initial position x_0. For a given U_0 and V(x), the integral is mass independent. Generalizing to three dimensions, two different ions with the same charge, kinetic energy, and initial desorption angle have the same trajectories Their times-of-flight are strictly proportional to the square root of the mass. Therefore, it is possible to compare kinetic energies of different ions using a time-of-flight detector even with an imperfect electric field configuration. In practice, where U_0 is much less than the drift tube voltage, ions have very similar trajectories.

In the idealized PSD detector, the ion travels through a region of uniform field of distance d_1 and through a drift region of distance d_2 before reaching the microchannel plates. The time in the acceleration region can be written

$$t_1 = \frac{1440\ m^{1/2}}{q\ E}\ [(U_0\cos^2\theta+qV)^{1/2} - (U_0\cos^2\theta)^{1/2}]\ , \qquad (2)$$

where t_1 is the time (ns), m the ion mass (amu), q the charge (integer), E the field (volts/cm), U_0 the initial kinetic energy (eV), θ the initial desorption angle from normal, and V the drift tube voltage. When $U_0 << qV$,

$$t_1 \sim \frac{1440\ m^{1/2}\ d_1}{(q\ V)^{1/2}}\ . \qquad (3)$$

The time resolution δt_1 for a distribution of U_0 and θ is

$$\frac{\delta t_1}{t_1} \sim \frac{1}{(q\ V)^{1/2}}\ \delta\ [(U_0\ \cos^2\theta\ )^{1/2}\ ] \qquad (4)$$

when $U_0 << qV$.

The time in the drift region is

$$t_2 = 720\ d_2\ \frac{m^{1/2}}{(q\ V + U_0)^{1/2}} \qquad (5)$$

with a resolution of

$$\frac{\delta t_2}{t_2} \sim \frac{\delta(U_0\ \cos^2\theta)}{2(q\ V + U_0\ \cos^2\theta)} \qquad (6)$$

where again $U_0 << qV$.

Let us use Eqs. 2-6 with typical experimental values to obtain a time-of-flight distribution. For use later in comparing to experiment, let us assume d_1 = 1.38 cm, d_2 = 5.72 cm, and V = 1677 volts. The time-of-flight of $^7Li^+$ desorbing normal to the surface with an initial kinetic energy U_0 of 2 eV is about 390 ns. With a distribution U_0= 4-0 eV normal to the surface, we obtain t_1 = 122.5-128.6 ns and t_2 = 265.4-265.7 ns. Most of the broadening occurs in the acceleration region, yet the ions spend two thirds of the time in the drift region.

A time-of-flight analyzer could be used to obtain kinetic energy and angle distributions if the analyzer were equipped with a position-sensitive detector. To obtain quantitative distributions, it is desirable that the detector approach the ideal of a uniform electric field along the flight path so that Eqs. 1-6 can be used. I considered the feasibility of such a detector by comparing the results of a trajectory calculation, using the JASON and X-RAY programs,[4] with the "ideal" trajectories of Eqs. 2-6. The "unterminated" geometry, shown in Fig. 3 with calculated equipotential curves, consists of a sample and a detector microchannel plate array. The electric field configuration is improved in the "terminated" geometry (not shown) by adding a large back plane to the manipulator and a set of four appropriately-biased termination rings between the back plane and the microchannel plates. Times-of-flight of O^+ ions for the "ideal", "unterminated", and "terminated" geometries are shown in Table I. Ion times-of-flight for the "unterminated" geometry are shifted to lower

time from the ideal; displacements R are shifted badly. Even with the terminations and back plane, ion times-of-flight and displacements differ from the ideal by about 2 and 5 percent, respectively. Unfortunately, the calculated angles and kinetic energies are sensitive to small errors in time-of-flight and displacement R. To obtain quantitative ion kinetic energies and angle distributions, better agreement with the ideal configuration is required.

The angle-resolving time-of-flight analyzer has other design problems. For proper angular resolution, the desorption pattern on the microchannel plates must be much larger than the photon beam spot size, which at the Stanford Synchrotron Radiation Laboratory (SSRL) can be quite large (1x3 mm). This requires large microchannel plates (75 mm diameter) and long times-of-flight (to spread out the desorption pattern). However, the time-of-flight must be kept less than approximately 1 μs (because of the 780 ns pulse period of SSRL). H^+, being the lightest ion, is the best system for combined mass and angle resolution.

A combined angle-resolved and mass analyzer would have limited resolution in angle and kinetic energy. These limitations may not be a significant problem: theory, to date, does not provide a quantitative relationship between desorption angle and bonding configuration, and it is uncertain whether quantitative angular distributions would lead to new knowledge about surfaces. On the other hand, qualitative or semi-quantitative angular distributions have been instructive in adsorbate systems.[5]

The PSD mass spectrum from a freshly-cleaved LiF(001) crystal is shown in Fig. 4. (This spectrum is discussed in Chap. IV). The ion peaks have weak shoulders at higher times, probably resulting from ion scattering. A strong "prompt" signal (from light emitted from the crystal) occurs in coincidence with the synchrotron photon pulse. The peak width (2.7 ns full width at half maximum) of the prompt is a measure of the experimental timing resolution. Masses one through 21 arrive in the 780 ns time interval between synchrotron radiation pulses; masses 33±3 and 48±4 arrive as "wrap arounds".

The major peaks of the LiF mass spectum are replotted and compared to a simulated spectrum in Fig. 5. The times-of-flight are scaled by the square roots of the masses, which we showed earlier is a rigorous factor for ions desorbing with the same kinetic energy and angle. The $^6Li^+$ and $^7Li^+$ peaks are so similar that they follow a single curve, as is expected. The F^+ peak is very similar to (but not exactly the same as) the Li^+ peaks. The H^+ peak is shifted from Li^+ and F^+ to lower times, indicating the H^+ ions desorb with a higher initial kinetic energy. The scaled H^+ peak appears to be broadened as compared to the other peaks as an artifact of the 2.7 ns timing resolution.

The simulated mass spectrum of Fig. 5 was generated using Eqs. 2 and 5 with an assumed initial ion kinetic energy distribution. Pian's experimental kinetic energy distribution of ions[6] from LiF at 100 C is asymmetric with a peak at about 2.3 eV, but the detailed peak shape depends on surface charging. I chose a Gaussian with mean of 2 eV and

a FWHM of 1.6 eV to generate the simulated distribution. The distance d_1 was adjusted to force the peak to be at about 390 ns. The simulated peak is much too narrow, with agreement particularily poor at high kinetic energies, where the simulated spectrum drops sharply. Probably the largest factor in broadening the mass peaks (especially for a cleaved insulator) is non-idealities in fields.

C. Absolute Flux Measurements of Beam Line III-1 at the Stanford Synchrotron Radiation Laboratory

Absolute flux measurements on Beam Line III-1 at the Stanford Synchrotron Radiation Laboratory (SSRL) are documented in this Section. The operation of Beam Line III-1 itself has been described in detail previously.[7,8] These measurements were performed by D. Charleston of the SSRL staff in March of 1983 and have not been reported elsewhere. These results are used in Chap. V and Chap. VI and shall also be used in planned future publications.

The absolute flux of Beam Line III-1 per mA of current in the storage ring is shown in Fig. 6 for 50 μ monochromator entrance and exit slits. The relative photon flux between 50 and 750 eV was obtained by measuring gold photoyield from a gold photodiode and correcting for gold photoabsorption.[9] These relative flux measurements were normalized to the absolute flux between 50 and 250 eV, as measured using a National Bureau of Standards (NBS) Al-Al_2O_3 photodiode (NBS serial number 243, calibrated by NBS Sept. 1981, drift

< 3 percent per year). It should be stressed that these measurements are reliable only for a limited period of time. Flux above the C(1s) edge decreases substantially with beam exposure (over the course of several months) as carbon collects on optical elements. The flux measurements should not be used for before September 1982 or after October 1983 when the monochromator was re-aligned.

The monochromator on Beam Line III-1 has adjustable slits so that the photon energy resolution can be changed. Relative flux estimates for the 600 l/mm and 1200 l/mm gratings are shown in Table II for different slit settings. I estimated the relative photon fluxes at hν = 160 eV in Nov. 1982 for the 600 l/mm grating by measuring restoring current to a gold mesh with a picoammeter. Some relative flux measurements for the 1200 l/mm grating were compiled by R. Rosenberg based on data of Feb. and Dec. 1982. While all estimates could be refined considerably, I report them here because the relative fluxes have not been measured previously, to my knowledge. These relative fluxes may depend critically on monochromator alignment; thus Table II should not be used for before September 1982 or after October 1983 when the monochromator was re-aligned.

Table I. Results of trajectory calculations for 8 ev O^+ ions as described in text. θ is the initial desorption angle from the normal, R is the arrival position of the ion at the microchannel plate array, and t is the time-of-flight.

Ideal acceleration region

θ(deg)	R(cm)	t(ns)
0	0	500
15	0.127	501
75	0.493	520

Unterminated configuration

θ(deg)	R(cm)	t(ns)
0	0.049	468
15	0.168	470
75	0.545	486

Configuration with ground plate and 4 terminations

θ(deg)	R(cm)	t(ns)
0	0.007	492
15	0.134	492
75	0.496	511

Table II. Relative fluxes at Beam Line III-1 at the Stanford Synchrotron Radiation Laboratory versus entrance and exit slit settings (Winter 1982-1983).

600 l/mm grating, $h\nu$ = 160 eV

Slit Setting (μm)	Relative Flux
200	12
100	4
50	1
40	0.6
30	0.3
20	0.1
10	0.02

1200 l/mm grating, $h\nu$ = 395 and 525 eV

Slit Setting (μm)	Relative Flux
50	1
30	0.5
20	0.12
10	0.04

REFERENCES

1. D. J. Ruggieri, IEEE Trans. Nucl. Sci. NS-19, No. 3, page 74, (1972).

2. S. A. Fields, J. L. Burch, and W. A. Oran, Rev. Sci. Instrum. 48, 1076 (1977).

3. C. N. Burrous, A. J. Lieber, and V. T. Zaviantseff, Rev. Sci. Instrum. 38, 1477 (1967).

4. S. Sackett and R. Healey, "JASON — a Digital Computer Program for the Numerical Solution of the Linear Poisson Equation," Lawrence Radiation Laboratory report UCRL-18721, (1969), unpublished.

5. T. E. Madey, F. P. Netzer, J. E. Houston, D. M. Hanson, and R. Stockbauer, in Proceedings of the First International Workshop on Desorption Induced by Electronic Transitions (DIET-1), (Williamsburg, Virginia, 1982), edited by N. H. Tolk, M. M. Traum, J. C. Tully, and T. E. Madey (Springer-Verlag, Berlin, 1983), page 120.

6. T. R. Pian, Ph.D. Thesis, University of Wisconsin—Madison (1982) unpublished.

7. J. Stöhr, "Instruction Manual for the New Grasshopper Monochromator", (1980), unpublished.

8. F. C. Brown, R. Z. Bachrach, and N. Lien, Nucl. Instrum. and Meth. 152, 73 (1978).

9. R. H. Day, T. Lee, E. B. Saloman, D. J. Nagel, Los Alamos Report LA7941-MS, (1981), unpublished.

FIGURE CAPTIONS

Fig. 1 Schematic of the time-of-flight mass spectrometry technique including the photon source, photon beam monitor (labeled as "I_0 Signal"), sample, detector, and associated electronics.

Fig. 2 Drawing of the PSD time-of-flight mass spectrometer and the time structure of the synchrotron radiation.

Fig. 3 Calculated equipotentials for the "unterminated" PSD detector geometry. Positive ions originate from the front face of the grounded sample and are accelerated towards a microchannel plate array biased at -3000 volts, which contains the detector elements. The boundary around the detector and sample is grounded to simulate the chamber walls. The sample, microchannel plate array, and boundary have cylindrical symmetry about the z axis.

Fig. 4 Time-of-flight mass spectrum of ions desorbing from a LiF(001) surface.

Fig. 5 Scaled times-of-flight of H^+, $^6Li^+$, $^7Li^+$, and F^+ from a LiF(001) surface are compared to a simulated spectrum. In the simulated spectrum, ions desorbed normal from the sample with a Gaussian kinetic energy distribution with mean of 2.0 eV and a full width at half maximum of 1.6 eV.

Fig. 6 Absolute photon fluxes from Beam Line III-1 at the Stanford Synchrotron Radiation Laboratory (SSRL) in March 1983. The plots were digitized from data provided by D. Charleston of the SSRL staff. The storage ring electron energy was 1.5 GeV. The monochromator entrance and exit slits for the 600 and 1200 l/mm gratings were set at 50 μm. These measurements apply to the period between September 1982 and October 1983.

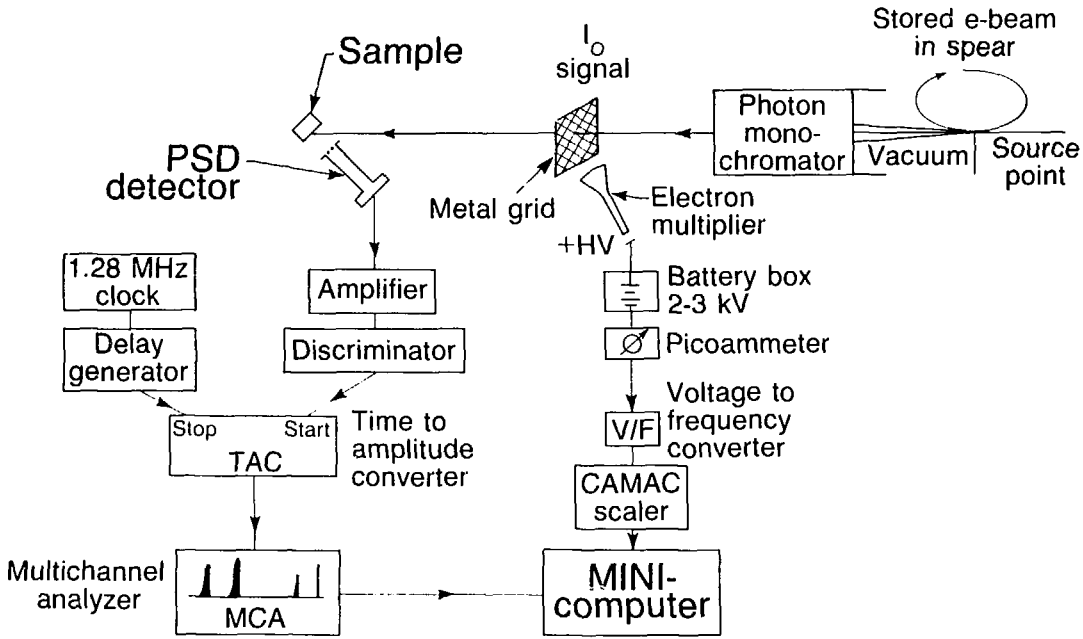
Sample
I_o signal
Stored e-beam in spear
Photon mono-chromator
Vacuum
Source point
PSD detector
Metal grid
Electron multiplier
+HV
1.28 MHz clock
Amplifier
Battery box 2-3 kV
Delay generator
Discriminator
Picoammeter
Stop
Start
TAC
Time to amplitude converter
Voltage to frequency converter
V/F
CAMAC scaler
Multichannel analyzer
MCA
MINI-computer
XBL 838-3132

Figure 1

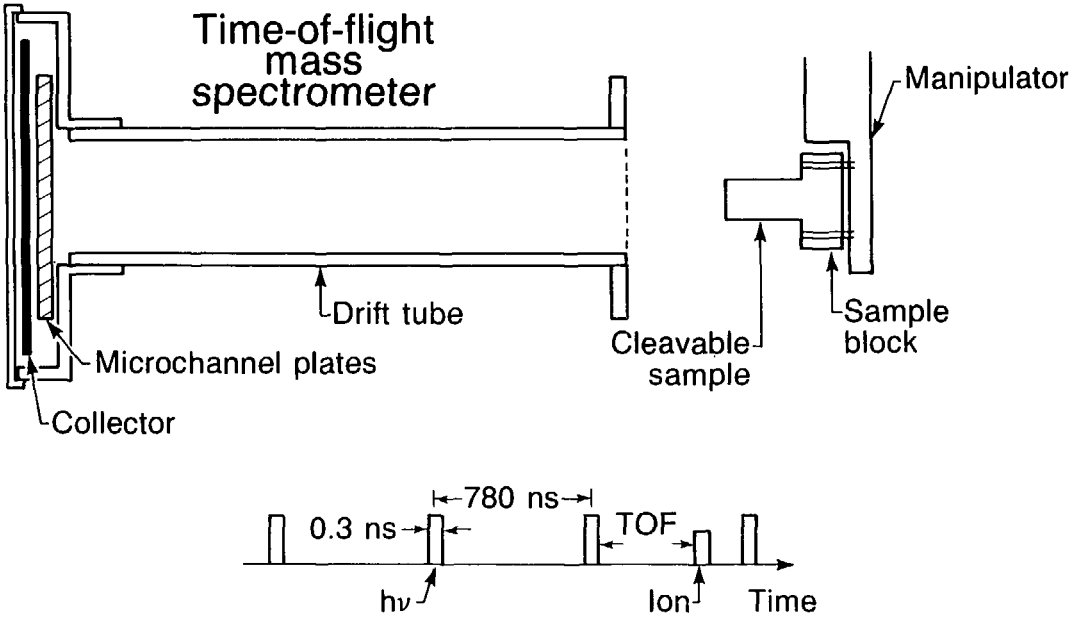

XBL 838-3131

Figure 2

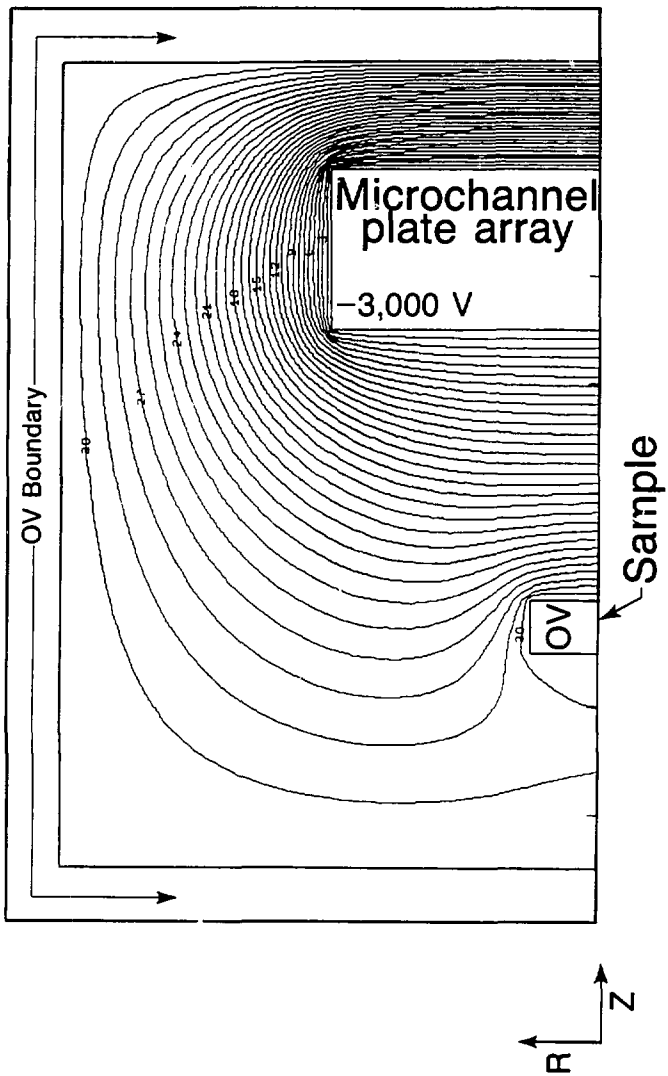

XBL 838-3133

Figure 3

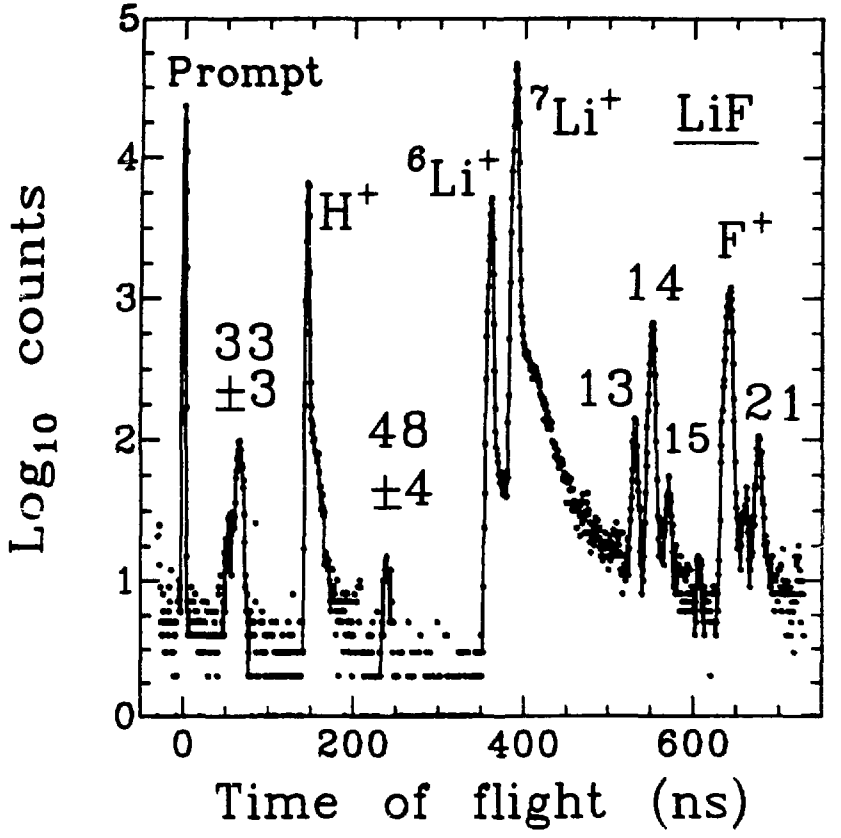

XBL 8310-11917

Figure 4

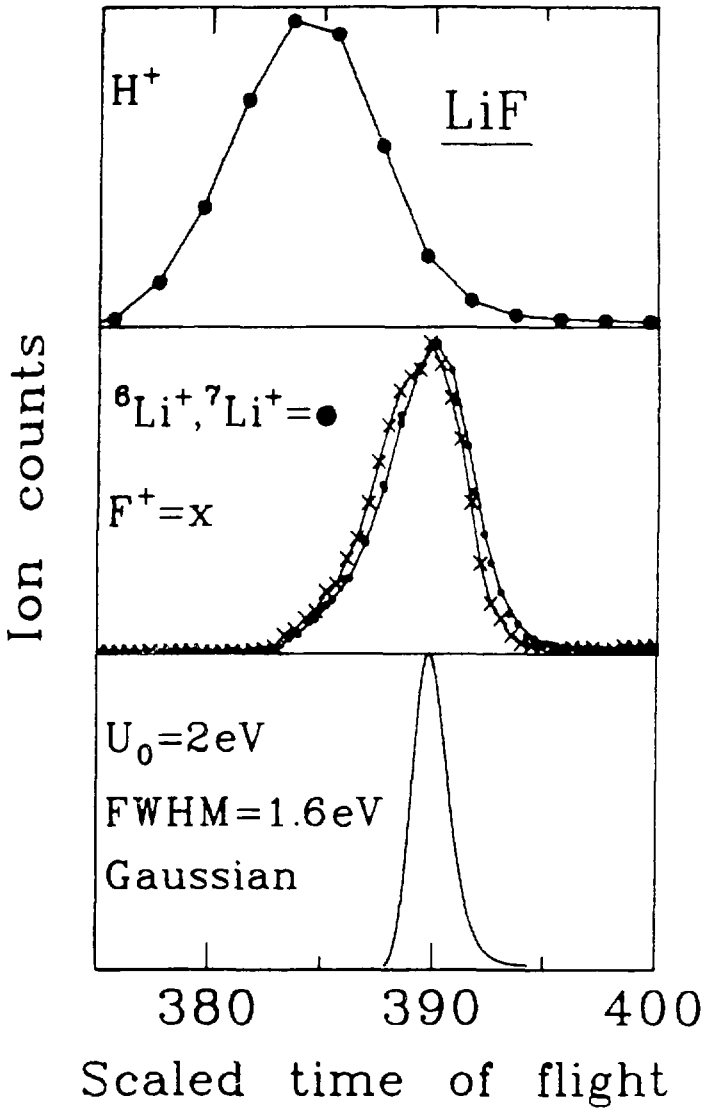

XBL 8310-11918

Figure 5

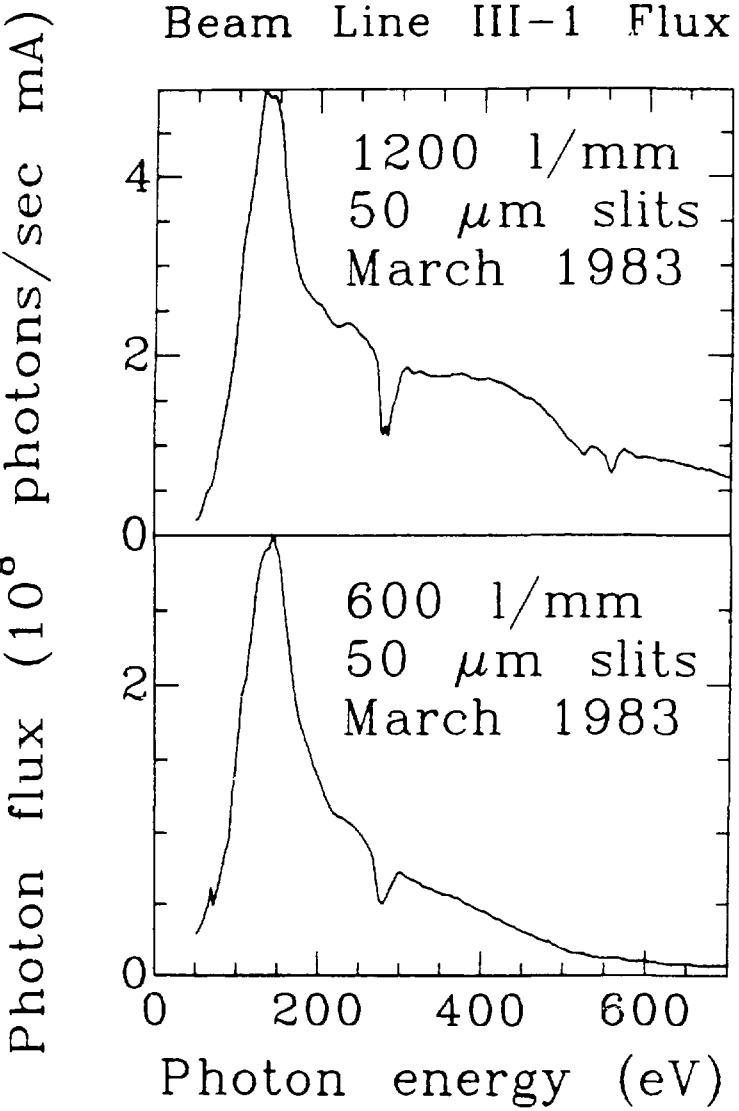

XBL 8310-11916

Figure 6

III. THE AUGER DECAY MECHANISM IN PHOTON-STIMULATED DESORPTION FROM SODIUM FLUORIDE*

ABSTRACT

Photon-stimulated desorption of Na^+ and F^+ occurs from a NaF(100) cleaved surface upon Na(1s) excitation. These measurements represent the first observation of metal cation desorption following metal cation core excitation. In agreement with the Auger decay model of desorption, both sodium and fluorine positive ion yields (versus photon energy) are similar to total electron yield in the vicinity of the Na K-edge, except for a pre-edge peak observed predominantly in Na^+ desorption. Intra-atomic Auger decay of the Na(1s) core hole followed by charge transfer from adjacent halogens is shown to initiate desorption. The resulting neutral or positively charged halogens provide the driving force for desorption of sodium ions from the surface. Expressions are developed for the maximal energy available to the desorbing Na^+ or F^+ ions.

A. Introduction

Photon-stimulated desorption (PSD) from ionic materials has been shown to occur by ionization of surface-atom core levels followed by Auger relaxation of the core hole.[1] Charge transfer of two or more electrons from the bonding region accompanies the Auger decay cascade, and a surface anion species may become positively charged. If the repulsive multihole final state is sufficiently long lived,[2,3] the species may be expelled as a positive ion from the surface. In this Chapter a description of this mechanism, Auger-stimulated desorption (ASD), is developed to encompass both metal-cation and halogen-anion species desorbing as positive ions. We shall identify the major channels in the Na(1s) Auger decay cascade resulting in desorption and derive equations for the maximal energy available to the desorbing Na^+ and F^+ ions.

Alkali halides have advantages as systems for studying the ASD mechanism. Since the absolute electron-energy thresholds[4] for electron-stimulated desorption (ESD) of ions are high (18 eV for NaCl), ion desorption by secondary-electron ESD should be much less important than the direct ASD mechanism. The ionicity[5] of sodium fluoride and other alkali halides is about 90%, justifying the use of simple bonding concepts. Both anions and cations desorb as positive ions from alkali halides, allowing useful comparisons. Clean samples are prepared easily by cleavage in vacuum.

Alkali halides also have complicating features. Calculations predict surface distortions on the order of 5% of a lattice spacing in

alkali-halide and other surfaces.[6-11] The stoichiometry of vacuum-cleaved surfaces may be different from that of the bulk: Gallon et al. cleaved alkali-halide crystals and monitored the desorbed species with a mass spectrometer.[12] About one atomic plane of fluorine desorbed from lithium fluoride within 10 seconds after cleavage; lithium also desorbed. Both sodium and fluorine desorb from NaF after cleavage. Exposure to radiation can alter the surface. X-rays produce F centers and other defects in alkali halides. Neutral halogens desorb upon low-energy-electron bombardment,[13,14] enriching the metal content of the surface. At electron and photon energies corresponding to substrate core levels, excited neutral-metal atoms desorb with high intensites, yielding atomic line radiation.[15,16] Since our intent in this work is to develop the Auger decay model for highly ionic systems, we defer discussion of the complex role of defects and hydrogen in ion desorption from alkali halides.

Experimental methods are described in Section B. Results are presented and described, under four subsections - yield spectra, the pre-edge feature, mechanisms, and energetics — in Section C. In Section D, the major conclusions are summarized.

B. Experimental

The experiment was performed at beam line III-3 at the Stanford Synchrotron Radiation Laboratory (SSRL) using photons of energies between 1075 and 1155 eV. The monochromator[17] transmitted a flux of $2x10^9$ photons/sec with a resolution of about 0.7 eV full width at half maximum (FWHM) at 1100 eV. The sodium fluoride crystals, of optical quality, were cleaved *in situ* at a pressure of $4x10^{-10}$ torr. To minimize charging, the sides of the crystals were coated with colloidal graphite. The PSD experiments were conducted with the light in p polarization at an incident angle of 45^0, and employed a time-of-flight mass spectrometer described elsewhere[1] with a modified drift tube designed to avoid saturation of the microchannel plates. This drift tube, biased between -500 and -1500 V to accelerate the ions, was equipped with two masks and electrostatic deflectors, allowing ions to pass while restricting line of sight between sample and microchannel plates. Total-electron-yield measurements used a positively biased channeltron electron multiplier. The ion- and electron- yield spectra were normalized to incident photon flux as measured by electron yield from a graphite-coated grid.

C. Results and Discussion

In this section, yield spectra, the pre-edge structure, mechanisms, and energetics are discussed separately.

1. Electron- and Ion- Yield Spectra at the Na K-edge

Ion and electron yields from a cleaved NaF(100) sample are plotted against photon energy in Figs. 1 and 2. Fig. 1 covers a photon-energy range of 80 eV, while Fig. 2 displays a 20-eV range near threshold in more detail. The sums of several scans are shown in the prethreshold region in Fig. 2. The intensity ratio of Na^+:F^+:H^+ is about 4:2:7. The electron-yield spectra have the same threshold and gross features as the ion-desorption curves. In Fig. 1 an absorption spectrum[18] of a 20000Å NaF film evaporated by K. Rule shows qualitative agreement with the other spectra and with another published absorption spectrum.[19] Our monochromator was calibrated by shifting the electron-yield peaks and valleys to match these two absorption spectra; an error of ± 0.5 eV was estimated in matching these peaks. The valley at 1083 eV is slightly deeper for electron yield and H^+ yield than for Na^+ and F^+ yield. A snarp structure (~ 1.3 eV FWHM) occurs as a resolved peak in Na^+ about 2.3 eV below the inflection point of the electron-yield threshold. The intensity and position of the peak are approximately the same for a freshly cleaved surface as for a surface exposed to the photon beam for many hours. The feature is at least 3 times as weak, if present at all, in F^+, and is absent in H^+ and electron yield.

Assuming a photon flux of 2×10^{9} photons/sec (Ref. 17) and 20% detector efficiency, about 3×10^{-8} Na^{+} ions desorb per photon at the Na^{+}-yield maximum. With the use of Ne or Na photoionization cross sections[20,21] (~ 2×10^{5} barns) and arbitrarily considering ionization of only the surface atomic layer, approximately 10^{-4} Na^{+} ions desorb per surface ionization. By comparison, yields of excited alkali neutrals desorbing from alkali halides are several orders of magnitude larger than ion yields.[15]

In photoabsorption of alkali ions in alkali halides the ionic environment of the alkali ion produces a barrier in the potential of the photoexcited electron. In the approach of Dehmer and Åberg,[22] the barrier partitions the final states into two classes -- inner-well (exciton) states and outer-well states. The exciton states have free-ion character and are embedded in the continuum of the outer-well states. For Li(1s) absorption[23-25] in LiF, the first prominent structure, assigned to core excitons, lies several eV below the conduction band minimum. However, for Na(1s) absorption in NaF, the first large peak at 1077.7 eV may lie near the conduction band[19] edge: in the rigid-band approach the Na(1s) level to conduction band transition energy is between 1076.4 and 1078.6 eV (depending on the choice[26-30] of literature values). The rigid-band approach has been discussed previously,[25] and gives a reasonable estimate of the position of the conduction band[23,24] minimum for Li(1s) absorption in LiF.

In ASD the ion yield is directly proportional to the core-hole

creation rate. Electrons from direct photoexcitation, Auger and exciton decay, and electron scattering contribute to the total-electron yield. Because of electron-electron scattering and multiplication, secondary electrons resulting from Auger decay may predominate over those resulting from near-threshold photoelectrons. The charge-transfer process in ASD occurs over a short range and the ions are believed to originate exclusively from the surface layer; the photoionized species responsible for total-electron yield can be many lattice spacings from the surface.[31] Both the ion-yield and the Auger decay component of the total-electron yield are strictly proportional to the absorption cross section and can be compared directly, but the ion yield is more surface sensitive than the electron yield. Assuming that ASD is the primary desorption mechanism, the lack of significant differences (excluding the pre-edge structure) between the PSD and electron yield indicates that the surface sites responsible for PSD are probably similar in electronic structure to those of the bulk.

2. Pre-edge structure in Na^+ desorption

An assignment of the pre-edge structure at 1073.5 ± 0.5 eV must account for both preferential Na^+ desorption and the position and shape of the peak. The following possibilities can be rejected.

(1) The high-absolute-energy ESD threshold[4] for Na^+ desorption from NaCl eliminates single ionization of a halogen and other low-energy processes as channels for exclusive Na^+ desorption

from NaCl and, by analogy, from NaF.

(2) A step or edge site (i.e. a site with a low surface Madelung potential) is expected[28,32] to have a greater $Na^+(3s^{-1}) \rightarrow Na^{2+}(1s^{-1}\ 3s^{-1})$ binding energy than a bulk site; ionization of such a surface site cannot account for a pre-edge structure.

(3) Atomic Hartree-Fock calculations with relativistic corrections were performed on Na and Na^+ using the code of Froese Fischer[33] as modified by Cowan;[34] good agreement with the experimental 1s binding energy[35] and the 1s → 3p Rydberg energy was found (i.e. ± 0.5 eV) for excitation from the neutral-sodium ground state. The calculated $Na^+(1s^2 2s^2 2p^6)\ ^1S$ to $Na^+(1s^1 2s^2 2p^6 3p)\ ^1P$ energy difference is 1078.6 eV; a core-exciton transition energy may be within a few eV of the corresponding free ion transition energy. (In LiF, the Li 2p exciton is 0.3 eV lower[25] than the corresponding experimental transition energy of the free ion.) Therefore, the pre-edge peak at 1073.5 eV is unlikely to be derived from a Na^+ 1s → 3p Rydberg transition.

The dipole-forbidden transition to the $Na(1s^1 2s^2 2p^6 3s)$ state, estimated to have a transition energy of 1072.54 eV in an unrestricted Hartree-Fock calculation[36] of the NaF_6^{5-} cluster, is a possible assignment for the pre-edge structure. A dipole-forbidden Li^+ 1s → 2s exciton is observed in LiF, allowed[24] by coupling to odd-parity phonons. For preferential Na^+ desorption to result, however, the transition would have to occur exclusively on surface sodium ions; it is unknown whether this would be the case.

Defects might give rise to absorption below the main edge. A standard bulk defect is a halogen vacancy. Excitation of a Na(1s) electron to produce an F center in such a site, however, may have a low cross section and may not result in preferential Na^+ desorption. Sample cleavage may result in a nonstoichiometric surface in which sodium atoms are present; electron bombardment can reduce Li in certain lithium salts.[37,38] Sodium metal itself[18] has a low-energy absorption edge (1071.7 eV) and a broad structure after threshold unlike any features in the NaF spectrum. However, if the sodium atoms are isolated on the NaF host lattice, their absorption spectra may more closely resemble the spectrum[35] of atomic Na, which has a sharp dominant Na 1s → 3p Rydberg peak at 1074.9±0.3 eV followed by weaker structures. For the Na^+ pre-edge peak to correspond to this atomic transition, a shift of about -1.4 eV would be required. The Hartree-Fock 3p Rydberg rms orbital radius in Na($1s^1 2s^2 2p^6 3s3p$) is 2.6Å, while the NaF lattice nearest-neighbor distance[39] is 2.317Å; we speculate that the transition may therefore only appear in the surface layer and be perturbed in the bulk. A pre-edge Rydberg-type structure has also been observed[40] in D^+ desorption from D_2O ice. For this Na 1s → 3p Rydberg-type assignment to be plausable, subsequent decay of the core hole must occur such that Na^+ is produced in a repulsive state on the surface; it is not known whether such a repulsive state will be produced.

3. Auger Decay Mechanism

ASD (Refs. 41,42) accounts for anions being converted to positive ions and then desorbing, with thresholds at both anion and cation core levels. Following halogen-ion photoabsorption in an alkali halide, the halogen decays by the Auger process, becoming positively charged. This positively charged species then experiences a repulsive Madelung potential, and desorbs with a few eV kinetic energy. Following metal-ion photoabsorption the core hole decays with an interatomic charge-transfer step, producing a positively charged halogen which desorbs as before. Although the Auger effect itself is usually regarded as intra-atomic in nature, this latter interatomic decay process has often been represented as interatomic Auger decay. The decay mechanism has been considered previously only in general terms, and has been limited to understanding anions desorbing as positive ions. In the discussion below we shall describe a model for the desorption of both Na^+ and F^+ ions following an interatomic process of Na(1s) hole decay in which the initial Auger step itself is intra-atomic.

Experimental evidence for interatomic Auger decay from core levels is limited. Linewidth broadening originally attributed to interatomic decay was later assigned[43] to phonon broadening. Interatomic Auger decay energies for several ionic systems[44] were estimated and compared to experimental spectra; several weak features were assigned to interatomic Auger decay in NaF. A rough comparison shows the area of the $Na(K)Na(L_{23})F(L_{23})$ structure of Ref. 44 to

be about 1% that of the intra-atomic Na($KL_{23}L_{23}$) ^1D structure. Transition rates for Auger decay have been calculated:[45] for solid CH_4 and CF_4, the intra-atomic rates are a factor of 10^4 larger than the interatomic rates; only for systems such as Na/O or Mg/O are the calculated inter and intra-atomic rates comparable. Clearly, interatomic Auger decay can be considered as a major decay channel only when the normal intra-atomic decay cannot take place.

In NaF, the Na(1s) hole produced by photoionization can decay, with a low probability, via a Na(K)F(L)F(L) or Na(K)Na(L)F(L) process, or with much higher probability by an ordinary Na(KLL) intra-atomic decay. If we consider the latter channel, Na^{3+} is produced within 10^{-15} sec (the initial state being Na^+). Charge transfer from surrounding fluorine ions must then occur, by the process

$$Na^{3+} + F^- \rightarrow Na^{2+} + F^0, \qquad (1)$$

exothermic by 53 eV, followed by either

$$Na^{2+} + F^0 \rightarrow Na^+ + F^+ \qquad (2)$$

or

$$Na^{2+} + F^- \rightarrow Na^+ + F^0 \qquad (3)$$

which are exothermic by 14 eV and 28 eV, respectively, as estimated using point-charge lattice corrections to free-ion energies. The energy released in the charge-transfer steps may result largely in

fluorescence or in expulsion of electrons from the valence band. The latter process has the net result of an interatomic Auger event; its probability is determined by the extent of polarization about the multihole sodium ion. The quasi-interatomic Auger decay $Na(L_3)F(L_3)F(L_3)$ is endothermic. The experimentally observed[44] quasi-interatomic Auger decay $Na(L_3)F(L_3)F'(L_3)$, where F and F' are different fluorines, is exothermic by ~ 7 eV.

These processes, Eqs. (1)-(3), should proceed on a very fast time scale, leaving the sodium ion that had lost a 1s electron back in its original charge state, as Na^+, with at most a little excitation energy in the outer shell. The net result, after about 10^{-12} sec (a vibrational period) is either that two of the nearest-neighbor fluorine atoms will be neutral F^0, or that one will be unipositive F^+. In either case the total electrostatic environment of the Na^+ ion in question can be repulsive, leading to desorption of the Na^+ ion (or of course the F^+ ion could desorb).

The real issue to be resolved in discussing this mechanism is therefore not whether the Na^+ ion can desorb by Na(1s) photoionization at the Na K-edge, but the subtler question of whether the electrostatic environment can remain repulsive long enough for this desorption to occur, i.e., for 10^{-12} sec or longer. Electronic polarization of the lattice will occur within about 10^{-15} sec, and will partially screen the repulsive terms in the potential. The effectiveness of this screening depends on the extent of the polarization. Diffusion of the two excess positive charges (on two F^0 atoms

or one F^+) away from one other will be much slower; in a completely ionic material it could occur only by electron hopping, while faster charge transfer through bonds is feasible in a more covalent material. Thus the polarizability and ionicity can both be critical in establishing the feasibility of positive-ion desorption in ionic lattices such as alkali halides.

4. Ion-Desorption Energetics

In the limit of complete ionicity, we can readily derive the energies available to both the metal and halogen atoms desorbing as positive ions. Following the approach of Mott and Littleton[46,47] for an ionic lattice in which one anion site is made neutral or positively charged, we combine electrostatic attraction and repulsion, Born repulsion, and polarization relaxation to determine the net repulsion energy. This total repulsion energy can be transferred either to the lattice or to a desorbing ion or both. It thus represents the maximal energy available to a desorbing ion. Unfortunately, a comparison of the repulsion energy to experimental kinetic energies[4] is obviated by the presence of surface charging. The approach taken below may thus be especially valuable in predicting ionic species that cannot desorb by a given process.

Consider Na^+ desorbing from a sodium chloride lattice site, in which z electrons have been removed from a neighboring halogen ion. We choose NaCl, although the energetics of NaF are very similar. The net energy E^+ available for desorption of Na^+ is the difference

between the repulsive energy U^+ resulting from an effective charge z on the neighboring halogen and the cohesion energy W^+ of the Na^+ ion to the lattice. All quantities are defined as positive in sign. The repulsion energy U^+ is

$$U^+ \sim \frac{z\,e^2}{r\,k_{eff}} , \tag{4}$$

where e is the electron charge, r is the distance between the Na^+ and the halogen under consideration, and k_{eff} is the effective dielectric constant. For a maximal estimate of repulsive energy, we set k_{eff} equal to 1. For a nearest neighbor, with[39] r = 2.820Å, we find U^+ to be about 5.1 z, measured in eV, for NaCl. The cohesive energy W^+ to remove a Na^+ ion from the surface is

$$W^+ = \alpha\, E_M^+ - E_{BR}^+ - 0.5\, e\, \phi^+ - E_S^+, \tag{5}$$

where α is the surface correction to the bulk Madelung energy E_M^+. For Na^+ in a perfect (100) surface lattice site[48] $\alpha = 0.96$ and $E_M^+ = 8.92$ eV. The second term E_{BR}^+ is the Born repulsion energy, about 1 eV for NaCl. The polarization potential[46] ϕ^+ in a rigidly held lattice is about 1.5 eV for NaCl; if the removal is on a time scale such that the lattice can relax, the polarization term is about 3.5 eV. For desorption, the time scale is intermediate but closer to the relaxed lattice case. If we ignore the surface correction E_S^+ to the Born repulsion and polarization terms, then

W^+ is about 4.3 eV. The net energy $E^+ = U^+ - W^+$ for desorption of a Na^+ ion is

$$E^+ = U^+ - \alpha E_M^+ + E_{BR}^+ + 0.5\, e\, \phi^+ + E_S^+ . \qquad (6)$$

Production of a positive halogen ion corresponding to z = 2 is clearly sufficient to expel a Na^+ ion from the surface. We see that U^+ and W^+ are comparable if we maximize the contribution of U^+ by setting the dielectric constant equal to 1 for single ionization of a halogen ion. If this latter process could lead to metal-cation desorption, Na^+ would have a low energy threshold at the halogen np binding energy. However, the ESD absolute threshold energy[4] at 18 eV for Na^+ desorption from NaCl is too high, eliminating this possibility for NaCl.

The energy E^- available to a desorbing positive halogen ion is

$$E^- = \alpha E_M^- + E_{BR}^- - 0.5\, e\, \phi^- - E_S^- . \qquad (7)$$

For alkali halides, the bulk Madelung energy E_M^- and surface correction α have the same values as those of the cation. The Born repulsion term E_{BR}^- for the positive halogen ion has a smaller value than that of the cation. The polarization term ϕ^- has two contributions: (1) When the halogen atom X is ionized to X^+, the lattice relaxes, stabilizing the halogen in the lattice, and (2) as the halogen is removed, polarization stabilizes the vacancy,

facilitating removal of the halogen. If the first term is more important, ϕ^- will be positive in sign. E_S^- is the surface Born repulsion and polarization correction term.

Surface Madelung energies (αE_M) of many step sites are between 50% and 70% of the bulk values and energies of other sites are even lower.[48] The Madelung-energy term provides the driving force to desorb the halogen ion, making desorption of halogens from majority (high surface Madelung energy) sites favored energetically. For metal cations, which are repelled from a neighboring ionized halogen, yet bound to the lattice by the Madelung interaction, desorption from minority (step, edge, and other) sites is favored.

D. Conclusions

ASD accounts for Na^+ and F^+ desorption from NaF. Following photoabsorption of the Na K-shell, the sodium ion decays via the KLL Auger process. Relaxation of the Na^{3+} species to the original charge state Na^+ occurs primarily by charge transfer from surrounding fluorines. The net result after about 10^{-12} sec is that either two of the nearest-neighbor fluorine atoms will be F^0, or that one will be F^+. The electrostatic environment of the F^+ ion and the neighboring Na^+ ions can be repulsive, leading to desorption. The leading term for energies available to the desorbing ions are the surface Madelung energy (α E_M) and the electrostatic repulsion U, respectively. In particular, desorption of the halogen is preferred energetically from majority surface sites, while metal cation desorption is preferred energetically from minority sites. In order for desorption to occur the electrostatic environment must remain repulsive for a characteristic time: This time will be controlled by the diffusion rate of the two holes (on two F^0 or one F^+) away from each other. In fact, the efficiency of the desorption process, about 10^{-4} Na^+ ions desorbing per surface ionization, is small. The ASD model predicts the observed ESD absolute thresholds [the Cl(3s) edge at 18 eV for Na^+ desorption[4] from NaCl, and the F(2s) edge at 32 eV for F^+ desorption[49] from LiF], the observation of halogen and metal species desorbing as positive ions, and the general agreement of the ion-desorption spectra to the total electron yield in NaF. In chapter IV some limitations of this model are demonstrated.

ACKNOWLEDGMENTS

The authors wish to acknowledge useful discussions with D. R. Jennison. The work was supported by the Naval Weapons Center Independent Research Fund, the U.S. Office of Naval Research, and the Director, Office of Energy Research, Office of Basic Energy Sciences, Chemical Sciences Division of the U. S. Department of Energy under Contract No. DE-AC03-76SF00098. Sandia National Laboratories is supported by the U.S. Dept. of Energy under contract number DE-AC04-76-DP00789. Experiments were conducted at the Stanford Synchrotron Radiation Laboratory, supported by the NSF through the Division of Materials Research.

REFERENCES

*Paper published with co-authors Z. Hussain, D. A. Shirley, M. L. Knotek, G. Loubriel, and R. A. Rosenberg, Phys. Rev. B 28, 4793, 1983.

1. M. L. Knotek, V. O. Jones, and V. Rehn, Phys. Rev. Lett. 43, 300 (1979).
2. P. J. Feibelman, Surf. Sci. 102, L51 (1981).
3. D. E. Ramaker, C. T. White, and J. S. Murday, J. Vac. Sci. Technol. 18, 748 (1981).
4. T. R. Pian, Ph.D. thesis, University of Wisconsin—Madison, 1982 (unpublished).
5. J. A. Van Vechten, Phys. Rev. 182, 891 (1969).
6. S. Sawada and K. Nakamura, J. Phys. C 12, 1183 (1979).
7. M. A. Van Hove and P. M. Echenique, Surf. Sci. 88, L11 (1979).
8. M. A. Van Hove and P. M. Echenique, Surf. Sci. 82, L298 (1979).
9. Y. W. Tsang and L. M. Falicov, Phys. Rev. B 12, 2441 (1975).
10. G. C. Benson and T. A. Claxton, J. Chem. Phys. 48, 1356 (1968).
11. G. C. Benson, P. Balk, and P. White, J. Chem. Phys. 31, 109 (1959).
12. T. E. Gallon, I. G. Higginbotham, M. Prutton, and H. Tokutaka, Surf. Sci. 21, 224 (1970).
13. P. D. Townsend, R. Browning, D. J. Garlant, J. C. Kelley, A. Mahjoobi, A. J. Michael, and M. Saidoh, Radiat. Eff. 30, 55 (1976).
14. H. Overeijnder, M. Szymonski, A. Haring, A. E. de Vries, Radiat.

Eff. 36, 63 (1978).

15. N. H. Tolk, M. M. Traum, J. S. Kraus, T. R. Pian, W. E. Collins, N. G. Stoffel, and G. Margaritondo, Phys. Rev. Lett. 49, 812 (1982).

16. T. R. Pian, N. Tolk, J. Kraus, M. M. Traum, J. Tully, and W. E. Collins, J. Vac. Sci. Technol. 20, 555 (1982).

17. Z. Hussain, E. Umbach, D. A. Shirley, J. Stöhr, and J. Feldhaus, Nucl. Instrum. Methods 195, 115 (1982).

18. K. C. Rule, Phys. Rev. 66, 199 (1944).

19. A. A. Maiste and R. E. Ruus, Opt. Spectrosk. (USSR) 46, 197 (1979).

20. I. M. Band, Yu. I. Kharitonov, and M. B. Trzhaskovskaya, Atom. Data Nucl. Data Tables 23, 443 (1979).

21. G. V. Marr and J. B. West, Atom. Data Nucl. Data Tables 18, 497 (1976).

22. T. Åberg and J. L. Dehmer, J. Phys. C 7, L278 (1974).

23. A. Zunger and A. J. Freeman, Phys. Rev. B 16, 2901 (1977).

24. M. Piacentini and J. Anderegg, Solid State Commun. 38 191 (1981).

25. S. T. Pantelides, Phys. Rev. B 11, 2391 (1975).

26. S. P. Kowalczyk, L. Ley, F. R. McFeely, R. A. Pollak, and D. A. Shirley, Phys. Rev. B 9, 381 (1974).

27. S. P. Kowalczyk, L. Ley, F. R. McFeely, R. A. Pollak, and D. A. Shirley, Phys. Rev. B 8, 3583 (1973).

28. P. H. Citrin and T. D. Thomas, J. Chem. Phys. 57, 4446 (1972).

29. W. H. Strehlow and E. L. Cook, J. Phys. Chem. Ref. Data 2, 163

(1973).

30. R. T. Poole, J. G. Jenkin, J. Liesegang, and R. C. G. Leckey, Phys. Rev. B 11, 5179 (1975).

31. W. Gudat and C. Kunz, Phys. Rev. Lett. 29, 169 (1972).

32. C. S. Fadley, S. B. M. Hagstrom, M. P. Klein, and D. A. Shirley, J. Chem. Phys. 48, 3779 (1968).

33. C. Froese-Fischer, Comput. Phys. Commun. 1, 151 (1969).

34. R. D. Cowan and J. B. Mann, Jr., J. Comput. Phys. 16, 160 (1974).

35. M. H. Tuilier, D. Laporte, and J. M. Esteva, Phys. Rev. A 26, 372 (1982).

36. A. B. Kunz, J. C. Boisvert, and T. O. Woodruff, J. Phys. C 15, 5037 (1982).

37. T. Sasaki, R. S. Williams, J. S. Wong, and D. A. Shirley, J. Chem. Phys. 69, 4374 (1978).

38. L. S. Cota Araiza and B. D. Powell, Surf. Sci. 51, 504 (1975).

39. M. P. Tosi, in Cohesion of Ionic Solids in the Born Model, Vol. 16 of Solid State Physics, edited by F. Seitz and D. Turnbull, (Academic Press, New York, 1964).

40. R. A. Rosenberg, P. R. LaRoe, V. Rehn, J. Stöhr, R. Jaeger, and C. C. Parks, Phys. Rev. B 28, 3026 (1983).

41. P. J. Feibelman and M. L. Knotek, Phys. Rev. B 18, 6531 (1978).

42. M. L. Knotek and P. J. Feibelman, Phys. Rev. Lett. 40, 964 (1978).

43. P. H. Citrin, P. Eisenberger, and D. R. Hamann, Phys. Rev. Lett. 33, 965 (1974).

44. P. H. Citrin, J. E. Rowe, and S. B. Christman, Phys. Rev. B 14,

2642 (1976).

45. J. A. D. Matthew and Y. Komninos, Surf. Sci. 53, 716 (1975).

46. N. F. Mott and M. J. Littleton, Trans. Faraday Soc. 34, 485 (1938).

47. N. F. Mott and R. W. Gurney, Electronic Processes in Ionic Crystals (Oxford University Press, London, 1946).

48. L. Piela and J. Andzelm, Surf. Sci. 84, 179 (1979).

49. J. A. Schultz, P. T. Murray, R. Kumar, Hsin-Kuei Hu, and J. W. Rabalais, in: Proceedings of the First International Workshop on Desorption Induced by Electronic Transitions (Williamsburg, Virginia, 1982), edited N. H. Tolk, M. M. Traum, J. C. Tully, and T. E. Madey (Springer-Verlag, Berlin, 1983).

FIGURE CAPTIONS

Fig. 1 Comparison of Na^+, F^+, H^+, and electron yield to the absorption spectrum of K. Rule (Ref. 18). Curves are drawn through the data as a visual aid.

Fig. 2 Comparison of total electron yield to Na^+, F^+ and H^+ desorption. Sums of several scans are shown in the pre-threshold region of the ion-desorption spectra. Curves are drawn through the data as a visual aid.

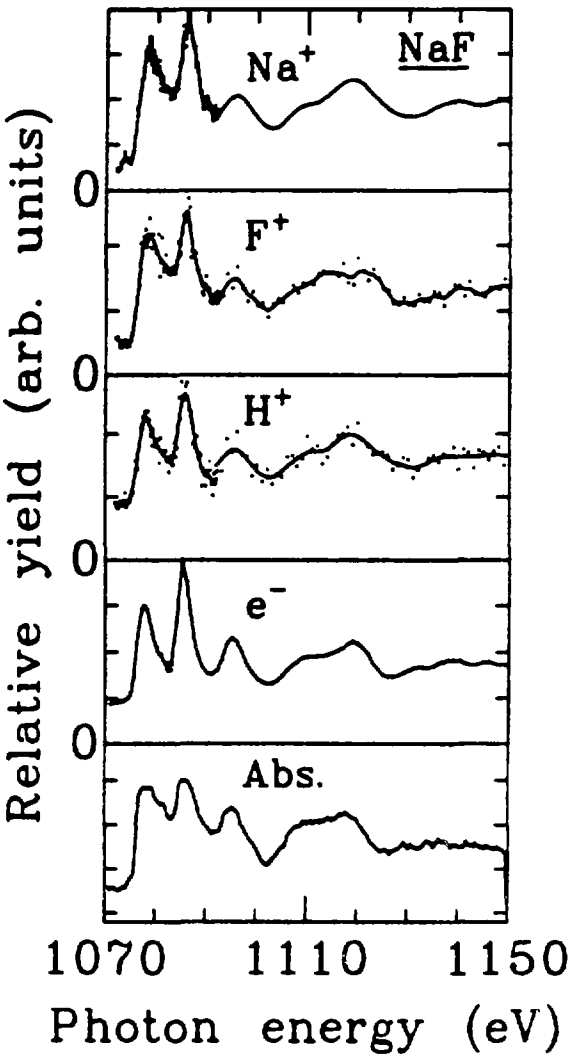

XBL 836-10082

Figure 1

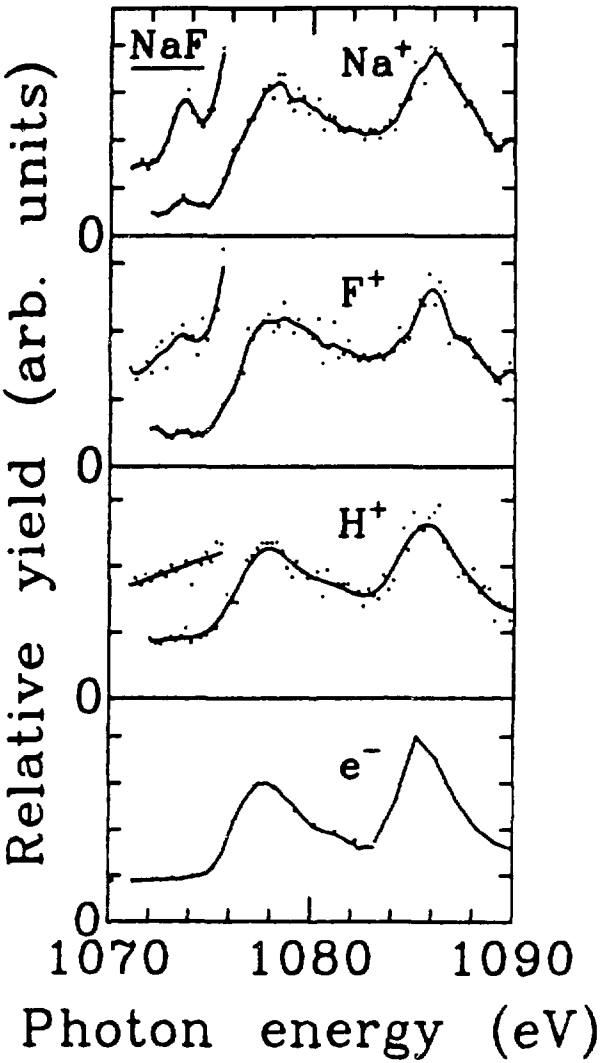

XBL 836-10083

Figure 2

IV. BEAM EXPOSURE DEPENDENCE AND MECHANISMS OF PHOTON-STIMULATED DESORPTION FROM ALKALI FLUORIDES*

ABSTRACT

Photon-stimulated desorption experiments were performed on the (001) face of LiF for photon energies near the F(2s) and Li(1s) edges (from 37 to 72 eV). There are structures in the F^+ yield above the F(2s) edge which are absent in the Li^+ spectrum, differences in detail in the Li^+ and F^+ yields near the Li(1s) edge, and considerable broadening of the desorption yields as compared to the bulk photoabsorption spectrum. The first observation of a strong x-ray, and visible, beam exposure dependence of ion yields from LiF and NaF is also presented. These results are discussed in terms of electronic and defect properties of alkali halides.

A. Introduction

Photon-stimulated desorption (PSD) of ions from alkali halides occurs following ionization of core levels.[1-3] In the Auger decay mechanism of desorption,[4,5] ionization of surface-atom core levels is followed by an Auger decay process involving the loss of two or more electrons from the valence band. The resulting multihole final state may be repulsive, and surface alkali or halogen species may desorb as positive ions. Because both alkali and halogen ion desorption result from the repulsive states produced by the Auger decay, their yields should be almost identical functions of photon energy and should strongly resemble the photoabsorption spectrum. In fact, the Na^+ and F^+ yields from NaF are very similar to photoabsorption near the Na(1s) edge.[3] Ion and excited neutral desorption near the Li(1s) level of LiF have been studied previously, but without mass resolution.[1] In this Chapter, ion yields and photoabsorption are compared in detail at the F(2s) and Li(1s) edges of LiF. Our intent is to test the applicability of the Auger decay model in the best-studied of the alkali fluorides.

We shall also describe a strong dependence of alkali and hydrogen ion yields from alkali fluorides on x-ray beam exposure. The H^+ yield from freshly-cleaved LiF and NaF crystals grows with total x-ray beam exposure. The Na^+ yield from NaF increases with intense polychromatic light but falls back to normal in the presence of visible light or monochromatic x-rays. Ion yields from NaF behave a if a single surface photoabsorption event could create PSD-active H^+

sites or destroy PSD-active Na^+ sites over an area of ~ 10^4 lattice sites. We propose mechanisms to account for this behavior. For instance, we propose that a photon activates a hydrogen species in the bulk, which migrates to the surface and is desorbed as H^+ by a subsequent photon.

Experimental methods are described in Section B. In Section C, the ion desorption spectra and photoabsorption are compared at the F(2s) and Li(1s) edges. In Section D, the beam exposure measurements from the LiF and NaF crystals are described and discussed. Conclusions are summarized in Section E.

B. Experimental

The experiments were performed on Beam Line III-1 at the Stanford Synchrotron Radiation Laboratory, using a "grasshopper" monochromator with a 600 line/mm grating. Charging was minimized by coating the sides of the samples with graphite before insertion in the vacuum chamber. Optical-quality NaF and LiF single crystals were cleaved in situ along the (001) plane at a pressure of 5×10^{-10} torr. The linearly-polarized synchrotron radiation was incident at 45^0 from the normal along the crystalline $[10\bar{1}]$ direction, so that the sample normal bisected the angle defined by the photon propagation and polarization directions. The positive ion and "prompt" photon yields were collected normal to the samples, using a time-of-flight analyzer with a drift tube biased between -1000 and -1500 volts. The prompt yield is a 2.6 ns full width at half maximum (FWHM) peak occuring in coincidence with the synchrotron light pulse. The analyzer detects only positive ions and photons, and has negligible efficiency[6] for photons below 7 eV. A 1500 Å aluminum window was inserted in the beam for all spectra between 37 and 72 eV to reduce second and higher order light. The ion- and prompt- yield spectra were normalized to the incident photon flux as measured by the electron yield from a graphite-coated grid. Absolute flux measurements performed subsequently[7,8] with a National Bureau of Standards photodiode were used to estimate yields as counts per photon and to estimate x-ray exposures. The zero order beam used in the beam exposure measurements consisted of both visible and x-ray light. As an approximate measure

of relative x-ray flux, the total electron yield from gold from the zero order beam was 1600 times that from 160 eV radiation; this value was used in estimating exposures. A 0.5 mw He/Ne laser (Spectra Physics Model 155) was used to determine the effects of visible light on ion yields. The laser is monochromatic at 632.8 nm (1.96 eV), but has contaminant discharge light (estimated to be less than 10 μW) in the blue and green.[9] No attempt was made to prevent light from entering the chamber through viewports. After the experiment, the crystals were removed and examined carefully; no obvious coloration was seen. (The electron-beam damaged LiF crystal had been re-cleaved, and could not be checked afterwards). The sodium fluoride cleaves were excellent; the lithium fluoride cleaves had some lateral fracture lines.

C. Li(1s) and F(2s) Ion Yield Spectra from LiF

In this Section we shall compare Li^+, F^+, and H^+ ion yields to bulk photoabsorption of LiF near the Li(1s) and F(2s) edges, and discuss our results in terms of the Auger decay mechanism. We shall also describe the effects of electron-beam exposures on the H^+ yield spectra.

The Auger decay model leads to several predictions. The following decay pathways can result in desorption: after Li(1s) photoionization, the Li(1s) core hole may decay by an interatomic Auger process to produce a positive fluorine ion.

$$Li^{2+} + F^- \rightarrow Li^+ + F^+ + e^- \quad . \tag{1}$$

The resulting electrostatic environments of both the F^+ ion and neighboring Li^+ ions are repulsive;[3] the F^+ ion itself or a neighboring Li^+ ion can therefore desorb exothermically. The dominant species of hydrogen present in alkali halides[10,11] are interstitial hydrogen atoms (H^0), H^- in halogen vacancies, and interstitial H_2. A decay process similar to Eq. 1 can lead to H^+ desorption of hydrogen from H^- or H^0 sites. For the H^- site, for instance, the Li-bonded H^- becomes positively charged and can be expelled from the lattice as H^+:

$$Li^{2+} + H^- \rightarrow Li^+ + H^+ + e^- \quad . \tag{2}$$

Following F(2s) excitation, an ordinary Auger decay

$$F^0(2s^1 2p^6) \rightarrow F^+ + e^- \qquad (3)$$

may lead to F^+ and Li^+ desorption. Neighboring H^- and H^0 species are spectators, and should not desorb as H^+. Therefore, we expect similar structures in Li^+ and F^+ desorption at the F(2s) and Li(1s) edges, and we expect those to resemble bulk photoabsorption. H^+ should have a threshold at the Li(1s) edge if Li-bonded hydrogen sites are present. We expect no H^+ yield threshold at the F(2s) edge if hydrogen is present only as H^0, H^-, and H_2.

In Fig. 1, we compare Li^+, F^+, H^+, and prompt yields from a LiF cleaved (001) surface to the photoabsorption spectrum of a thin evaporated film on an aluminum substrate, reported by Olson and Lynch.[12] The photon energy resolution in the ion and prompt yield spectra was between 0.64 and 1.1 eV FWHM in the photon energy range between 55 and 72 eV, while the resolution of the photoabsorption spectrum was 0.05 eV. Our LiF crystal was exposed to intense polychromatic (zero order) light during alignment. Our monochromator was calibrated by matching the prompt peak with those of previous photoabsorption[12-17] and reflection[18-20] peaks at 61.9 eV.

Photoabsorption near the Li(1s) threshold in LiF is well characterized. The shoulder at 60.8 eV and the prominent peak at 61.9 eV are assigned[21] to the $Li^+(1s \rightarrow 2s)$ and $Li^+(1s \rightarrow 2p)$ core excitons, respectively. The Li(1s) photoionization threshold[21]

occurs at 63.8±0.4 eV. The "prompt" photon yield spectrum from our cleaved crystal in Fig. 1 agrees closely with the bulk photoabsorption spectrum, although it lacks the dipole-forbidden, phonon-assisted $Li^+(1s \rightarrow 2s)$ exciton shoulder. We confirmed the lack of the shoulder at higher photon energy resolution (0.2 eV at $h\nu$ = 60 eV). The non-specular "prompt" signal had been interpreted previously as resonance fluorescence from the exciton and continuum states.[20] Because the prompt spectrum is bulk-derived, it serves as a useful internal calibration for the surface-derived ion yield spectra.

Contrary to our expectation that the ion yield and photoabsorption spectra should be similar, the ion yield spectra of Fig. 1 are considerably broader than the prompt or photoabsorption spectra. The three ion yield spectra are quite similar, differing mainly in the relative intensities of some of the features. For instance, the "peak" at 69.5 eV is much larger in the H^+ spectrum than in the other spectra. All ion spectra exhibit a double-peaked structure between 60.9 and 62.8 eV. That structure changes slowly with time or beam exposure. These spectra (and those of Fig. 2) were taken several days after cleavage but differ only in minor details from spectra taken 6 hours after cleavage. The F^+ spectrum has additional structures at 57.8 and 59.4 eV. If most of the ions desorbed from perfect (001) sites, we might expect the ion and photoabsorption spectra to be much more similar. The differences among the spectra (especially considering the broadening) are evidence that the desorption comes from complex minority sites or that the surface is

very rough.

In Fig. 2 ion yields are compared with prompt yield between the F(2s) and Li(1s) photoionization thresholds[21] at 38.2 ± 0.8 eV and 63.8 ± 0.4 eV, respectively. A broad structure above the F(2s) photoionization threshold between 40 and 45 eV occurs in the prompt and in the F^+ yields, but is absent in Li^+ or H^+ desorption. The Li^+ ion yield increases by a factor of twenty at about 60 eV, while the H^+ and F^+ yields increase by only a factor of 4. Our F^+ spectrum, and the absolute electron-stimulated desorption (ESD) threshold[22] for F^+ at about 34 eV, are consistent with an Auger decay mechanism of F^+ desorption following F(2s) or Li(1s) photoabsorption. The Auger decay mechanism is inconsistent with the lack of a Li^+ threshold corresponding to the F^+ threshold near the F(2s) edge. The large jump in yield near the Li(1s) edge is further evidence that Li^+ desorption is weakly coupled to channels below the Li(1s) edge, but strongly coupled to photoabsorption of the Li(1s) core hole. Therefore, F^+ probably desorbs by the Auger decay mechanism, while Li^+ does not.

The threshold in H^+ yield at the Li(1s) edge is consistent with desorption from Li-bonded sites. The nature of these sites changes with beam exposure: the H^+ structure near 61.9 eV is somewhat different in Fig. 2 (for a crystal which had less beam exposure) than the structure in Fig. 1. As discussed previously, the lack of a threshold at the F(2s) edge is consistent witn the Auger decay model: neutral or negatively-charged hydrogen is not expected to desorb as

H^+ following the F(2s2p2p) Auger decay. The H^+ yield is large below both the Li(1s) and F(2s) edges. Desorption below these edges could occur after single ionization of a Li-bonded hydrogen atom,

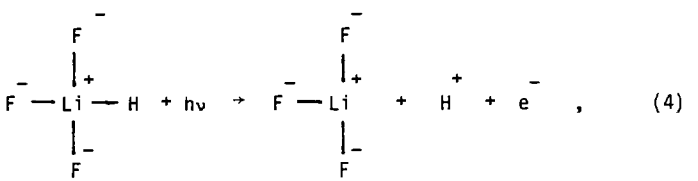

$$F^- - Li^+(F^-) - H + h\nu \rightarrow F^- - Li^+(F^-) + H^+ + e^- , \qquad (4)$$

where the ionized hydrogen atom desorbs by repulsion from the Li^+ ion. Incidently, the H^+ ions desorb with a higher kinetic energy than do Li^+ and F^+ ions at $h\nu$ = 62.8 eV: the $^6Li^+$, $^7Li^+$, and F^+ times-of-flight scale as the square roots of the masses as expected, but the H^+ ions arrive sooner than expected, as shown in Fig. 5 of Chapter II.

We studied the effects of electron-beam damage on the ion yields. Electron beam impact of alkali halides causes preferential desorption of halogen neutrals.[23,24] A surface plasmon loss peak observed on a vacuum-cleaved LiF (100) surface using characteristic loss spectroscopy indicates that a thin surface layer of neutral lithium accumulates with electron beam damage.[25] In Fig. 3, ion and prompt yield spectra are shown from a cleaved crystal exposed to a large (1000 eV, 6μA, 38 min) electron beam exposure. Notice the sharper edge structure in the Li^+ spectrum as well as the

dramatically changed H^+ spectrum. The prompt signal is unchanged as expected for a bulk process. The change in the H^+ spectrum must indicate formation of a new hydrogen surface species. Not surprisingly, all of the spectra differ from both Li metal[26] and lithium hydride[27,28] photoabsorption and fluorescence spectra.

D. Beam-exposure dependence of ion yields from NaF and LiF

Time-dependent effects were observed in PSD ion yields from both NaF and LiF. To explore these effects we have carried out systematic studies of the dependence of ion yields on beam exposure. Several crystals were cleaved in situ and were subjected to sequential irradiation by soft x-rays, zero-order light, and visible light. The results are presented below, in the spirit of reporting a survey of interesting phenomena. In general we cannot give unique explanations of these phenomena, but our observations set limits on the range of possible explanations, and plausible candidate mechanisms are hypothesized.

In Fig. 4 we plot ion yields from NaF in the first hour after cleavage. Monochromatic radiation (160 eV) was first allowed to strike the crystal at 7 minutes. The 160 eV photon energy was selected as the photon energy of maximum flux from the monochromator. This energy exceeds all but the K-shell binding energies of Na^+ and F^+ in NaF. The mass spectrum at 7 minutes showed weak (a few percent) peaks at masses corresponding to NaF^+ and Na_2F^+ as well as the H^+, F^+, and H^+ ion yields plotted in Fig. 4. The beam was shuttered at 38.5 minutes, and unshuttered again at 51.2 minutes. The 160 eV radiation flux[7,8] was approximately 10^{11} photons/(sec cm^2). The mean penetration depth is approximately 1000 Å, as estimated from atomic cross section data.[29,30]

Two important conclusions emerge from Fig. 4. First, variations in Na^+ and F^+ yields with beam exposure are easily observable.

These variations of ~ 10 percent are too large, relative to the cumulative surface depletion through desorption ($\leq 10^{-5}$ monolayers/min: an absolute upper bound based on assuming unity desorption of neutrals or ions per surface photoionization), to be attributable to gross changes in surface composition. Other explanations must be sought.

Second, the H^+ yield is clearly radiation-induced. It is also very large after sufficient exposure. Thus hydrogen-containing species must be both created by monochromatic (160 eV) radiation and readily desorbed by it, in two separate events. A plausible (but by no means unique) mechanism would involve a hydrogen species in the irradiated region of the bulk (ca. the first 1000 Å) being activated by irradiation, migrating to the surface and becoming trapped, and subsequently being ionized and desorbed by a second photon. For example, a U center (H^- in a halogen vacancy: a major form of hydrogen in alkali halides) could be converted to neutral hydrogen[10]

$$U \rightarrow H^0 + F , \qquad (5)$$

leaving an F center behind. This conversion could occur directly by photoionization or indirectly through loss of a loosely-bound electron on H^- to a nearby radiation-induced positive site. If the neutral H^0 migrated to the surface on a timescale of minutes and became trapped in a surface site, facile desorption as H^+ would be expected, following photon absorption via an Auger decay mechanism.

The timescale of minutes for migration of the slower H^0 species to the surface is inferred from the increase of H^+ yield following the dark period. This mechanism is consistent with the decreasing slope of the H^+ yield curve, which may imply saturation of active sites on the surface.

We tested the effects of large beam exposures by applying pulses of zero order (intense polychromatic) light and measuring the subsequent ion yields versus time under irradiation with 160 eV light. In Fig. 5 results are shown of the following exposure sequence: 160 eV light, darkness interrupted by a zero order pulse and a brief yield measurement at 160 eV, a long period of darkness, and further yield measurements at 160 eV. The zero order exposure was composed of soft x-rays (about 10^{16} photons/cm^2 as estimated using gold photoyield) and significant intensities of visible and ultraviolet light.

The initial decrease in H^+ yield followed by a slow rise to above the initial yield (seen in part in Fig. 5) is characteristic behavior following long zero order exposures. When shorter (20 sec) zero order exposures were applied, the initial decrease in H^+ yield did not occur, and the yield grew slowly from the initial value. According to the model described above, the initial decrease in yield would result from depletion of the surface active species (perhaps by desorption). The slow increase in H^+ yield would then occur as new PSD-active species diffused from the bulk to the surface.

The data in Fig. 5 establish several important facts concerning the Na^+ yield. First, the zero order exposure causes an enhancement

of the Na^+ yield. Second, the decay of the enhanced Na^+ yield is induced by the 160 eV light. The strength of this effect is surprising because five minutes of exposure to 160 eV light results in about 10^{11} surface photoionizations per cm^2. Therefore, it would appear that each surface photoionization would have to eliminate PSD-active species over an area of ~ 10^4 lattice sites to account for the observed decay. This latter observation eliminates a wide class of mechanisms from consideration in explaining the Na^+ yield enhancement.

Possible mechanisms for the enhanced Na^+ yield are restricted further by the observation that visible light also affects the Na^+ yield. We applied the following exposure sequence: 160 eV light, darkness, a zero order exposure, darkness, and a long period of 160 eV light during which the crystal was exposed three times to a 1.96 eV (red) laser. Fig. 6 shows the results: first, the decay curve of the Na^+ yield became more gradual as the total exposure of the crystal accumulated. Second, illumination with the laser quenched the enhanced Na^+ yield. The laser had only a slight effect on the Na^+ yield if no zero order light was applied previously.

The laser light interacts with the crystal by photoabsorption of a defect site. If the defect level lies close to the conduction band, photoconductivity can result. The laser photon energy is in a weakly absorbing region of the x-ray irradiated crystal photoabsorption spectrum, far from the F band (3.63 eV) and other color center bands.[31,32] If we use the published absorbance (0.114) of a heavily

x-ray irradiated (1.4 mm thick) NaF crystal[31] and our laser flux of 1.5×10^{15} photons per second, we estimate that an average of 10^8 photons are absorbed per atomic layer per second. Although this estimate is crude, it demonstrates that each 1.96 eV surface photo-absorption would have to eliminate PSD-active sites over an area of $\sim 10^6$ lattice sites to cause a substantial drop in yield.

A very speculative model consistent with some of the observations is the following: the band gap component of the zero order exposure produces mobile neutral sodium atoms which diffuse along the surface. The 160 eV photon creates a positively-charged trap (such as Na^{2+}) which stops a neutral sodium atom passing by, ionizes the atom, and ejects the sodium species as a positive ion (which is detected). The essential feature of this mechanism is that the Na^{2+} trap would effectively collect neutrals over a large area: a sodium atom with thermal kinetic energy travels several thousand Angstroms in 1 ns. This mechanism, while entirely speculative and dependent on the lifetime of the Na^{2+} species, would explain both the enhancement of the Na^+ yield and the low flux necessary to quench the enhanced yield. However, it is uncertain how the laser affects the Na^+ yield in this mechanism.

Another speculative approach is to assume that the enhanced Na^+ yield is associated with the space charge generated by the zero order light. The 160 eV and 1.96 eV radiation deplete this space charge by photoconductivity. Photoabsorption of many (10-100) layers would contribute to depletion of the space charge. The advantage of this

approach is that it provides a framework for understanding the effects of the laser. The crucial difficulty here is that we have no mechanism for understanding why the Na^+ yield might be enhanced from the space-charged crystal.

In summary, the PSD ion yields from NaF were strongly affected by irradiation. Controlled experiments enabled us to characterize the effects and to narrow down the range of possible explanations, but we were unable to develop a unique and complete model for the various observed phenomena.

Time-dependent ion yields were also observed from LiF. We exposed a LiF crystal to zero order light shortly after cleavage and monitored ion yields under irradiation with monochromatic light (62.8 eV). The 62.8 eV energy was selected as being the photon energy giving the highest ion yields from LiF. Yields of species desorbing from the crystal 15 and 69 minutes after cleavage are shown in Fig. 7. We assign several masses (13, 14, 21, 33, and 47 amu) to desorbing clusters rather than contaminant species because the ion yields decreased sharply with time, because we believe that our freshly-cleaved surface was clean, and because clusters have been observed to desorb previously from other alkali halides.[2] We can group these ion species according to time dependence. The ion yields of pure lithium clusters ($^7Li_2^+$, ^6Li-$^7Li^+$, and $^7Li_3^+$) decrease between 15 and 60 minutes by a factor of 100 or greater. In the second group, $^6Li^+$, $^7Li^+$, Li_2F^+, and F^+, ion yields decrease by factors ranging from seven to 1.4. In the third group, H^+,

Li_4F^+, and H_2^+, ion yields increase with time. In Fig. 8 we p[illegible] the time dependence of the H^+, $^7Li^+$, and F^+ ions. The time dep[illegible]ence of the H^+ and alkali ion yields is qualitatively similar in L[illegible]F and NaF.

Finally, we note that the effects of electron beam exposures on ion yields from alkali halides in ESD have been characterized previously. Pian et al. reported that alkali metal ion yields from NaCl increase with electron beam exposure.[2] We confirmed this increase in the Na^+ yield from NaF in PSD following a large (1 μA, 70 eV, 3 minute) electron beam exposure, and we observed a large decrease in H^+ yield.

E. Conclusions

We compared the ion yield spectra near the F(2s) and Li(1s) thresholds with photoabsorption from LiF. Thresholds in F^+ yield were found at both the F(2s) and Li(1s) edges, as is expected in the Auger decay model. However, in contradiction with the expectations of the Auger decay model, the Li^+ yield had no threshold at the F(2s) edge. A threshold in H^+ yield from LiF occured at the Li(1s) edge, which is expected if Li-bonded hydrogen atoms or negative ions are present. We suggested that single ionization of Li-bonded hydrogen atoms is responsible for the H^+ yield at 37 eV below the F(2s) and Li(1s) edges. All the ion yield spectra are considerably broadened in comparison to bulk photoabsorption at the Li(1s) edge, which is evidence that ion desorption comes from complex minority sites or that the surface is very rough.

Low-intensity x-ray and visible light exposures affect ion yields from cleaved LiF and NaF surfaces. The H^+ yield from freshly-cleaved LiF and NaF crystals grows as a function of total x-ray beam exposure. This growth in yield may result from conversion of hydrogen in the bulk (such as a U center) to a mobile form which migrates to the surface and is desorbed by a subsequent photon. Alkali metal ion yields (Li^+, Li_2^+, Li_3^+, and Na^+) from LiF and NaF increase upon exposure to polychromatic light. The enhanced yields drop back to normal in the presence of monochromatic x-rays or visible light (1.96 eV). While the mechanism for the enhanced alkali metal ion yields is unknown, a major conclusion of our study is that defect properties are

crucial in metal ion desorption from these alkali halides.

Acknowledgments

The authors acknowledge help in some of the experiments by L. Klebanoff and G. Kaindl. This work was supported by the Director, Office of Energy Research, Office of Basic Energy Sciences, Chemical Sciences Division of the U.S. Department of Energy under Contract No. DE-AC03-76SF00098. Sandia National Laboratories is supported by the U.S. Department of Energy under contract number DE-AC04-76-DP00789. It was performed at the Stanford Synchrotron Radiation Laboratory, which is supported by the Department of Energy, Office of Basic Energy Sciences and the National Science Foundation, Division of Materials Research.

REFERENCES

*Paper to be submitted for consideration for publication by Phys. Rev. B with co-authors G. Loubriel and D. A. Shirley.

1. N. H. Tolk, M. M. Traum, J. S. Kraus, T. R. Pian, W. E. Collins, N. G. Stoffel, and G. Margaritondo, Phys. Rev. Lett. 49, 812 (1982).
2. T. R. Pian, M. M. Traum, J. S. Kraus, N. H. Tolk, N. G. Stoffel, and G. Margaritondo, Surf. Sci. 128, 13 (1983).
3. C. C. Parks, Z. Hussain, D. A. Shirley, M. L. Knotek, G. Loubriel, and R. A. Rosenberg, Phys. Rev. B 28, no. 8, 1983.
4. P. J. Feibelman and M. L. Knotek, Phys. Rev. B 18, 6531 (1978).
5. M. L. Knotek, V. O. Jones, and V. Rehn, Phys. Rev. Lett. 43, 300 (1979).
6. Galileo Electro-Optics Corp., data sheet 4000B, May 1978 (unpublished).
7. D. Charleston, Stanford Synchrotron Radiation Laboratory, private communication, July 1983.
8. C. C. Parks, Ph.D. Thesis, University of California--Berkeley 1983 (unpublished).
9. R. Yazell, Spectra-Physics, Inc., private communication.
10. J. Schulman and W. Dale Compton, Color Centers in Solids, (Pergamon Press, Oxford, 1962).
11. P. D. Townsend and J. C. Kelly, Colour Centres and Imperfections in Insulators and Semiconductors (Crane, Russak, and Company, New York, 1973).

12. C. G. Olson and D. W. Lynch, Solid State Commun. 31 51 (1979).

13. W. Gudat, C. Kunz, and H. Petersen, Phys. Rev. Lett. 32, 1370 (1974)

14. A. A. Maiste, A. M.-É. Saar, and M. A. Élango, Fiz. Tverd. Tela (Leningrad), 16, 1720 (1974) [Sov. Phys. Solid State, 16, 1118 (1974)].

15. R. Haensel, C. Kunz, and B. Sonntag, Phys. Rev. Lett. 20, 262 (1968).

16. A. P. Lukirskii, O. A. Ershov, T. M. Zimkina, and E. P. Savinov, Fiz. Tverd. Tela (Leningrad) 8, 1787 (1966) [Sov. Phys. Solid State 8, 1422 (1966)].

17. W. Gudat and C. Kunz, in Proceedings of the IV International Conference on Vacuum Ultraviolet Radiation Physics, (Hamburg, 1974), edited by E. Koch, R. Haensel, and C. Kunz (Pergamon and Vieweg, Braunschweig, 1974), p. 392.

18. N. Kosuch, G. Wiech, and A. Faessler, ibid. p. 398.

19. K. Tsutsumi, O. Aita, K. Ichikawa, M. Kamada, M. Okusawa, and T. Watanabe, in Inner Shell and X-ray Physics of Atoms and Solids, edited by D. J. Fabian, H. Kleinpoppen, and L. M. Watson (Plenum, NY, 1981), page 775.

20. O. Aita, K. Tsutsumi, K. Ichikawa, M. Kamada, M. Okusawa, H. Nakamura, and T. Watanabe, Phys. Rev. B 23 5676 (1981).

21. A. Zunger and A. J. Freeman, Phys. Rev. B 16, 2901 (1977).

22. J. A. Schultz, P. T. Murray, R. Kumar, Hsin-Kuei Hu, and J. W. Rabalais in: Proceedings of the First International Workshop on

Desorption Induced by Electronic Transitions (Williamsburg, VA, 1982), edited by N. H. Tolk, M. M. Traum, J. C. Tully, and T. E. Madey, (Springer-Verlag, Berlin, 1983), page 191.

23. P. D. Townsend, R. Browning, D. J. Garlant, J. C. Kelley, A. Mahjoobi, A. J. Michael, and M. Saidoh, Radiat. Eff. 30, 55 (1976).

24. H. Overeijnder, M. Szymoński, A. Haring, A. E. de Vries, Radiat. Eff. 36, 63 (1978).

25. L. S. Cota Araiza and B. D. Powell, Surf. Sci. 51, 504 (1975).

26. T. A. Callcott, E. T. Arakawa, and D. L. Ederer, V International Conference on Vacuum Ultraviolet Radiation Physics, (Montpellier, 1977), edited by M. C. Castex, M. Pouey, and N. Pouey, 1 275 (1977).

27. A. A. Maiste, S. O. Cholakh, F. F. Gavrilov, and M. A. Élango, Fiz. Tverd. Tela (Leningrad), 16, 301 (1974) [Sov. Phys. Solid State, 16, 203 (1974)].

28. T. Miki, M. Ikeya, Y. Kondo, and H. Kanzaki, Solid State Commun. 39 647 (1981).

29. I. M. Band, Yu. I. Kharitonov, and M. B. Trzhaskovskaya, At. Data Nucl. Data Tables 23, 443 (1979).

30. G. V. Marr and J. B. West, At. Data Nucl. Data Tables 18, 497 (1976).

31. K. Konrad and T. J. Neubert, J. Chem. Phys. 47, 4946 (1967).

32. H. Blum, Phys. Rev. 128, 627 (1962).

FIGURES

Fig. 1. A comparison of Li^+, F^+, H^+ and prompt (PR.) yields to bulk photoabsorption (Ref. 12). The Li(1s) photoionization threshold at 63.8 eV, the $Li^+(1s \rightarrow 2s)$ exciton at 60.8 eV (short arrow), and the $Li^+(1s \rightarrow 2p)$ exciton at 61.9 eV (long arrow) are indicated in the absorption spectrum. Curves are drawn through the data a visual aid.

Fig. 2. A compa. .on of Li^+, F^+ and H^+ yields to prompt (PR.) yield. The F(2s) and Li(1s) binding energies at 38.2 and 63.8 eV, respectively are indicated in the prompt spectrum. Curves are drawn through the data as a visual aid.

Fig. 3. Li^+, H^+ and prompt (PR.) yield spectra of the electron beam damaged surface. The crystal was exposed to a 1000 eV, 6 μA electron beam for 38 minutes. Curves are drawn through the data as a visual aid.

Fig. 4. Na^+, F^+, and H^+ yields at 160 eV versus time after cleavage. The following exposure sequence was performed: dark (0–7 min), 160 eV (7–38.5 min), dark (38.5–51.2 min), 160 eV (51.2–59.2 min). For clarity one out of each five data points is enlarged.

Fig. 5. Na^+, F^+, and H^+ yields at 160 eV versus time after cleavage. The following exposure sequence was performed: 160 eV (410-420.8 min), dark (420.8-422.6 min), zero order (422.6-424.3 min), dark (424.3-426.0 min), 160 eV (426.0-426.9 min), dark (426.9-473.4 min), 160 eV (473.4-485 min). For clarity, one out of each four data points is enlarged.

Fig. 6. Na^+, F^+, and H^+ yields at 160 eV versus time after cleavage. The following exposure sequence was performed: 160 eV (550-559.8 min), dark (559.8-561.8), zero order (561.8-563.9 min), dark (563.9-565.9 min), 160 eV (565.9-595 min). During the latter period, three laser exposures occured: (575.4-576.2 min), (581.7-582.7 min), (587.6-588.6 min). For clarity one out of each three data points is enlarged.

Fig. 7. Time-of-flight mass spectra from a freshly cleaved LiF crystal 15 minutes (upper panel) and 69 minutes (lower panel) after cleavage. The exposure sequence was: dark and zero order (0-10 min), 62.8 eV (10-69 min). The prompt yield is labeled "PR." As discussed in the text, probable mass assignments are: 13 (^6Li-$^7Li^+$), 14 ($^7Li_2^+$), 15 ($^7Li_2H^+$ or CH_3^+), 21 ($^7Li_3^+$), 33 ($^7Li_2F^+$), and 47 amu ($^7Li_4F^+$).

Fig. 8. Li^+, F^+, and H^+ yields at 62.8 eV versus time after cleavage. The following exposure sequence was performed: dark and zero order (0-10 min), 62.8 eV (10-114 min), dark (114-144 min), 62.8 eV (144-200 min). Lines connect data points as a visual aid.

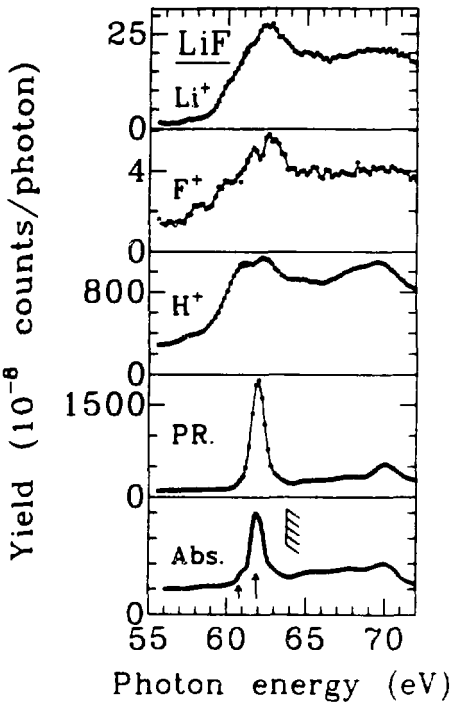

XBL 8310-11919

Figure 1

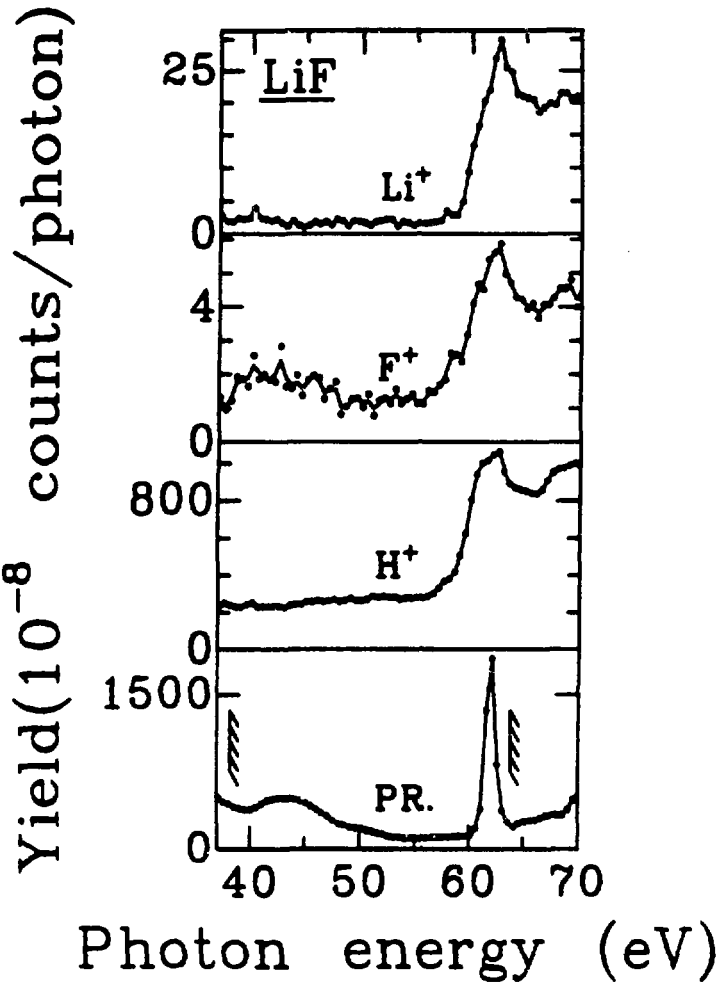

XBL 8310-11920

Figure 2

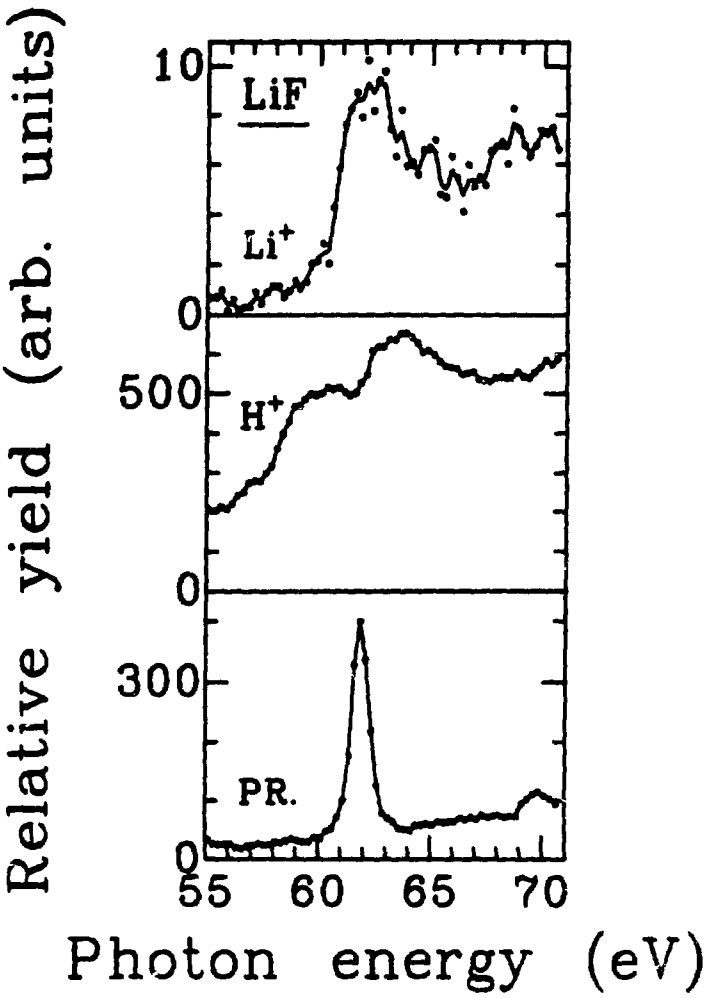

XBL 8310-11921

Figure 3

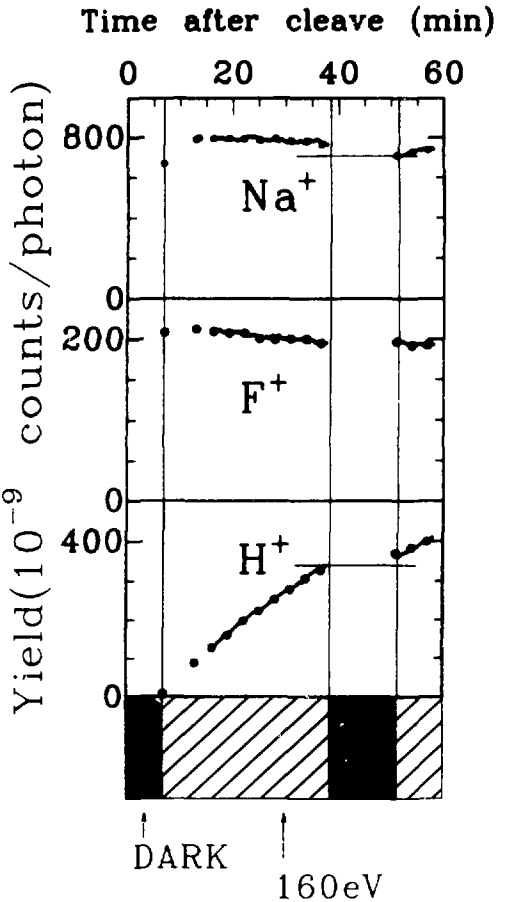

XBL 8310-894

Figure 4

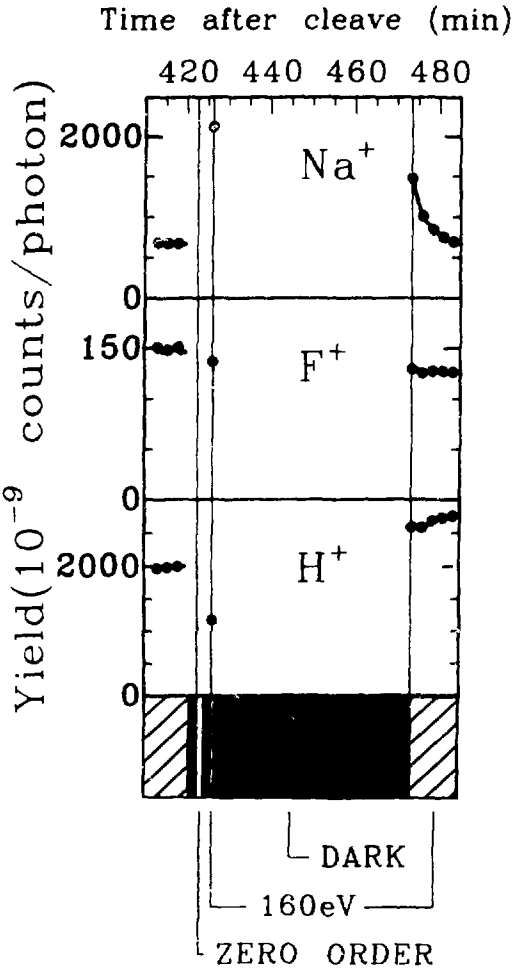

XBL 8310-895

Figure 5

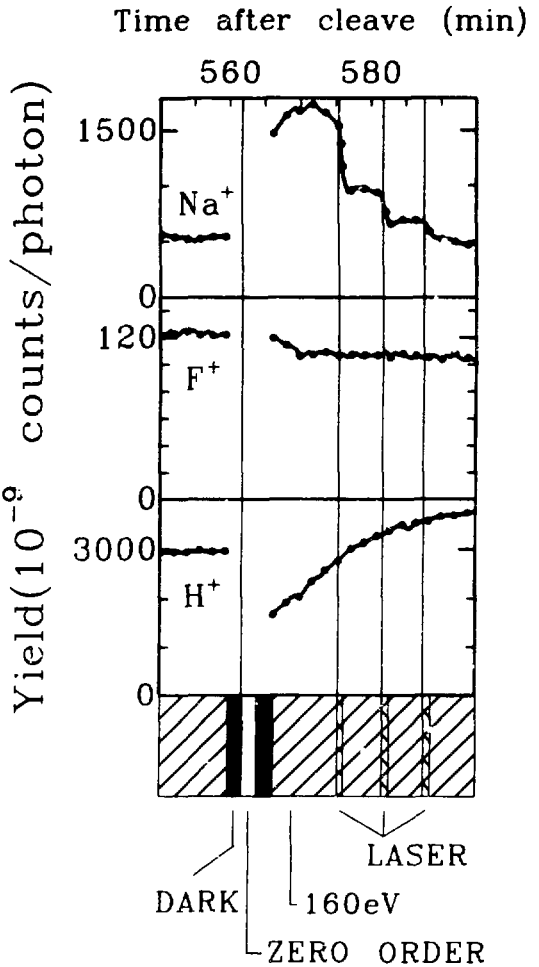

XBL 8310-896

Figure 6

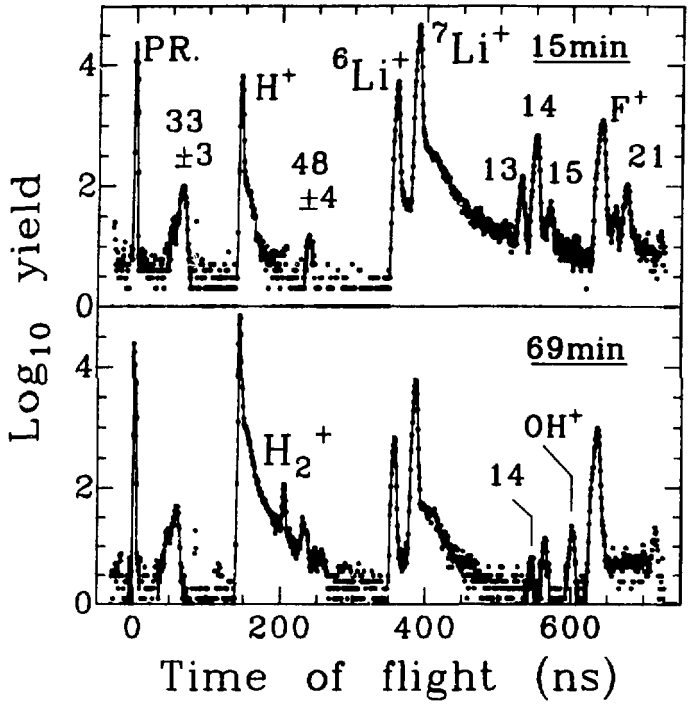
PR.
33
±3
H+
48
±4
6Li+
7Li+
15min
14
F+
13
15
21
69min
H2+
OH+
14
Log10 yield
4
2
0
0
200
400
600
Time of flight (ns)
XBL 8310-11922

Figure 7

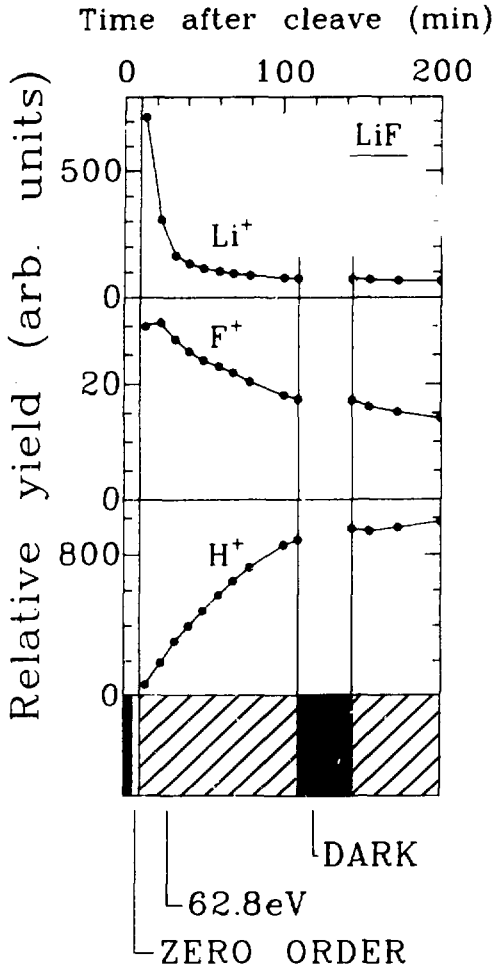

XBL 8310-897

Figure 8

V. INDIRECT MECHANISMS IN PHOTON-STIMULATED DESORPTION FROM CONDENSED MULTILAYERS

ABSTRACT

Photon-stimulated desorption of N^+ and O^+ ions from a condensed mixture of N_2 and O_2 was studied between the N(1s) and O(1s) edges. In a simple model ions desorb by photoabsorption followed by Auger decay and Coulomb explosion of the molecule that was photoionized. While reducing ion yields by delocalizing energy and trapping outgoing ions, the host lattice was presumed previously to be a spectator rather than a substantial contributer to desorption. In this study we find substantial N^+ desorption following O(1s) ionization, indicating that the photoionized molecule interacts strongly with the lattice and that an indirect mechanism of desorption is important. We consider the possibility of secondary electrons traveling through the lattice and desorbing ions. Using molecular cross sections, we find that this mechanism may be important and that the role of secondary electrons in ion desorption should be considered whenever ESD cross sections are in the range of 10^{-20} to 10^{-18} cm^2 or higher.

A. Introduction

Photon-stimulated desorption of ions from surfaces occurs following following core level photoabsorption. In the Auger decay mechanism of desorption, ionization of a surface-atom core level is followed by Auger relaxation of the core hole and localized charge transfer of two or more electrons from the bonding configuration.[1,2] The multihole final state can be repulsive, resulting in desorption of ions from the surface. Therefore, the ion yield varies in direct proportion to the photoabsorption cross section of the surface sites involved. In this mechanism, Auger-stimulated desorption (ASD), PSD has extreme surface sensitivity. ASD occurs as a desorption channel from many materials: alkali halides, metal oxides, condensed gases, and semiconductors.

A second ion desorption channel, in which the potential of PSD as a site-specific probe is lost, can predominate over ASD. At the N(K) and Ni(L) edges, Jaeger et al.[3,4] found a close correspondence of H^+ PSD and total electron yield as functions of multilayer thickness from a NH_3 film on Ni(100). As the NH_3 film was grown, the PSD and electron yield edge jumps decreased together at the Ni(L) edges, while the edge jumps rose together at the N(K) edges. If ASD were the only desorption mechanism, an edge jump should occur at the Ni(L) edge only with monolayer coverage, and the edge jump at the N(K) edge should remain constant with coverage. These results establish the major role of secondary electrons in desorbing ions, in a process called x-ray induced electron stimulated desorption (XESD). Jaeger

et al. estimated the contribution of XESD to be 60 percent, with the contribution of ASD being only 40 percent. Because a substantial fraction of excitations originate in the bulk, ion desorption is not proportional to surface photoabsorption. When XESD predominates, PSD has neglibible value as a surface probe.

To understand the roles of XESD and ASD more clearly, we studied N^+ and O^+ desorption from a thick N_2–O_2 film grown at 10–20 K. We found thresholds in N^+ and O^+ desorption at both the N(K) and O(K) edges. The O^+ threshold at the N(K) edge and the N^+ threshold at the O(K) edge unambiguously establish the importance of an indirect mechanism in desorption from this film. These results could be interpreted using an indirect, but still localized mechanism: photoabsorption and an Auger decay cascade, followed by charge transfer from a neighboring molecule, resulting in ion desorption of the neighbor. In view of Jaeger's results with ammonia films, however, it is more likely that XESD is the major indirect mechanism.

We shall show that indirect channels predominate in N^+ but not O^+ desorption. We consider whether XESD occurs largely by electron ionization of core levels or by ionization of valence levels. Desorption efficiencies, as measured by ions desorbed per ionization, are much higher following core hole ionization. On the other hand, secondary electrons at lower energy are more numerous and electron ionization cross sections of valence levels are higher. We shall find that valence excitation is more important in XESD.

A major unresolved question is whether XESD occurs mostly by low

energy electrons (10-50 eV) or by higher energy electrons (50-200 eV). If low energy electrons are most important, materials having high ESD absolute thresholds and low ESD cross sections at low energies will desorb mostly by direct mechanisms such as ASD. If intermediate or higher energy electrons are important, a major role of XESD from materials having high ESD cross sections must be contemplated. An experiment is suggested which may resolve this problem.

B. Experimental

The experiments were performed at the Stanford Synchrotron Radiation Laboratory on beam line III-1 at a resolution of 1.7 eV at 400 eV. Condensed films (hundreds of angstroms thick) were grown on a liquid-helium cooled alumina substrate in a chamber having a base pressure of 10^{-10} torr.[5,6] After completion of the initial film growth, the surface was refreshed by slow condensation of vapor from a doser tube, while keeping the chamber pressure below 10^{-9} torr. Ions were detected using a time-of-flight mass spectrometer employing a spiraltron to amplify the signal. The total electron yield (TEY) was measured using the same analyzer by biasing the spiraltron positively and measuring spiraltron collector current. All spectra were normalized to photon flux using electron yield from a gold mesh placed in the incident photon beam. Absolute measurements of ions per photon were performed using photon flux measurements taken subsequently with a National Bureau of Standards photodiode.[7,8]

C. Results

N^+, O^+, and total electron yields (TEY) from a thick condensed N_2-O_2 multilayer (N_2:O_2 ~ 1.35:1) are plotted versus photon energy near the N(K) and O(K) edges in Fig. 1. N^+, O^+, and electron yields increase sharply at both the N(K) and O(K) edges. N^+ desorption predominates over O^+ desorption between 395 and 590 eV, as measured by the edge jump, or difference in count rate above and below the N(K) and O(K) edges.

PSD has been performed on the pure N_2 and O_2 solids.[6,9] N^+ ion and electron yields near the N(K) edge from the thick N_2 multilayer were compared previously to gas-phase electron loss spectra[10] (ELS). The ion and electron yields are similar to, but broadened from, the gas phase ELS and photoabsorption spectra. The sharp peak at 400.96 eV in the gas phase, and in Fig. 1, is assigned[10] to a transition to the normally empty 2π molecular orbital. Peaks between 405 and 415 eV, completely broadened in Fig. 1, are assigned to Rydberg transitions. PSD occurs below the ionization threshold near 410 eV as expected in ASD or XESD. The ion yield spectra from condensed O_2 are also related to gas phase spectra, with a sharp 2π peak below threshold. Therefore, photoabsorption of these solids can be represented as predominantly molecular in nature, with effects of condensation as perturbations.

The mixture is composed of weakly-interacting molecular subunits; the spectra in Fig. 1 were fitted as a weighted sums of pure N_2 and O_2 ion or electron yields spectra. These fits are probably accurate

to 20 percent, which justifies the use of such a simple additive model of desorption. The edge jumps, or differential increases of yields, above and below the N(K) and O(K) edges were obtained. In Table I, these differential increases are expressed as counts per photon, ions per photon, and ions per surface ionization.

D. Discussion

We adopt the viewpoint that N^+ desorbing at the O(K) edge results from an indirect mechanism, while N^+ desorbing at the N(K) edge results from a combination of direct and direct mechanisms. From our data, we cannot distinguish between localized charge transfer or XESD as indirect channels. We shall emphasize XESD, because the predominance of XESD is established in NH_3 multilayers.

At 540 eV, N^+ desorbing by indirect channels predominated by a factor of 2.5 over total O^+ desorption, while at 420 eV, O^+ desorption by indirect channels was only 5-10 percent of total N^+ desorption. If we consider ions per surface ionization, O^+ desorption by indirect channels at the N(K) edge was about 10 percent of O^+ yield above the O(K) edge; the N^+ yield was comparable at both edges. The results cannot be explained entirely by assuming that N^+ merely has a greater propensity to desorb. These results indicate conclusively that indirect channels are a 10 percent effect for O^+ desorption, while being a much larger effect in N^+ desorption.

The contribution of XESD can be written as[4]

$$A^+ \sim [A]\,[B]\,\sigma_B(h\nu) \int \sigma_A(\varepsilon) D(h\nu,\varepsilon)\, d\varepsilon \qquad (1)$$

where A^+ is the ion yield of fragments of species A. We consider the differential increase of yield, or edge jump, at some edge of species B, which has an atomic or molecular photoabsorption cross section $\sigma_B(h\nu)$. The ESD cross section of A at an electron kinetic

energy ε is $\sigma_A(\varepsilon)$. The electron kinetic energy distribution in the solid as a function of ε is $D(h\nu,\varepsilon)$ for a particular photon energy $h\nu$. To include the contribution of all kinetic energies to XESD, the integral of the product of the latter two factors is taken. The yield is proportional to the surface concentration [A] of species A and and proportional to the concentration of B within the escape depth of the electrons.

In assessing the role of XESD in general, it is important to determine the electron kinetic energy range at which most of the XESD occurs. The onsets of ion desorption[6] in PSD from N_2 and other molecular solids at 20-30 eV are high. While not available from N_2 and O_2 solids, ion yields as functions of electron energy from adsorbate systems[11-14] rise slowly from high electron energy thresholds. The common picture from photoemission of the kinetic energy distribution, with a very large inelastic tail at low energies and rather small intensities at Auger and photoelectron energies, is misleading. These raw photoemission spectra must be corrected for analyzer transmission and losses in the grids; if this is done, the estimated contribution of higher kinetic energy electrons is ennanced.

Therefore, the XESD yield depends critically on the proportion of electrons having kinetic energies in the higher energy range where ESD cross sections are large. Because of the high ESD thresholds, condensed gases are unfavorable cases for XESD.

While ESD cross sections and electron energy distributions are not available, we can determine some essential aspects of XESD by

using molecular valence and K-shell photon and electron absorption cross sections. With this approach, we are limited to estimating the numbers of ionizations on the surface. We can relate ionizations to numbers of desorbing in a rough way using PSD results: the efficiency[8] of valence and K-shell ionization in PSD is about 10^{-6} and 10^{-3} ions per surface ionization, respectively.

Using the photon flux (7.2×10^{7} photons/s) and the O_2 molecular K-shell photoabsorption cross section[15-17] (0.5×10^{-18} cm^2), we estimate 3.6×10^{4} photoionizations per second occur per molecular layer at 540 eV. One O(KLL) Auger electron is produced per O(K) shell ionization, at an energy above the N(1s) binding energy. Using the N(1s) electron impact ionization cross section[18,19] ($<5 \times 10^{-20}$ cm^2) and assuming that Auger electrons from 10 layers contribute to electron ionization of the surface layer, we obtain about 20 surface N(1s) ionizations per second. If 10^{-3} ions desorb per surface ionization (as in PSD), a yield of only 0.02 ions per second is obtained from secondary K-shell ionization. The actual N^+ yield at 540 eV in Table I is 60 counts per second.

In Fig. 2, ionization cross sections by electron bombardment[20] are shown for N_2 and O_2 gases. Using 2.6×10^{-16} cm^2 as the electron cross section at 100 eV, one obtains a mean free path of 4 layers. (This value is greater that of the universal electron escape depth[21] of about 4 Å). The maximum number of secondary electrons per photon is $h\nu/\varepsilon$, where $h\nu$ and ε are photon and electron energies, respectively. Using 10 electrons per photon, a cross section of

$2x10^{-16}$ cm^2 for 50 eV secondaries, and $3.6x10^4$ photoionizations per second per layer, we obtain $7x10^4$ valence ionizations for each layer that contributes secondaries. If we grossly overestimate the flux of secondary electrons at the surface by assuming a total contribution of 20 layers, about 10^6 valence ionizations occur per second on the surface layer. To obtain the observed N^+ countrate in Table I of 60 counts per second, a desorption efficiency of 10^{-4} ions per ionization is required. In PSD, the efficiency at 32 eV is much lower, at 10^{-6} counts per surface ionization.

We can check this work in another way: as noted previously, the XESD source is on the order of $3.6x10^4$ ionizations per second per layer; again if we arbitrarily assume a contribution of 20 layers, we obtain a maximum electron flux of $7x10^5$ electrons per second through the surface. For the 60 counts per second N^+ signal in Table I to result from XESD, we need an ESD cross section of about 10^{-19} cm^2. ESD cross sections[22] for adsorbate systems are typically between 10^{-20} and 10^{-23} cm^2. For some adsorbate systems, higher ion desorption cross sections are known.[22,23]

Therefore, the estimated contribution of high energy O(KLL) Auger electrons in ionizing the N(1s) level is too low by a factor of 3000 to match the observed N^+ yield at 540 eV. This factor is large enough so that we have confidence in eliminating secondary K-shell ionization as a major channel in desorption. The valence shell estimates are more uncertain. The analysis does not explain why indirect channels are more important in N^+ desorption. In the

analysis above, we overestimated the numbers of secondaries and the numbers of layers contributing as sources of electrons. Even so, the ESD cross sections necessary for substantial XESD are on the high end of observed values for adsorbate systems.

E. Conclusions

We demonstrated that indirect mechanisms predominate in N^+ desorption from a condensed N_2-O_2 mixture. This is proved because about 2.5 N^+ ions desorb per O^+ ion following O(1s) photoionization and because N^+ yields per surface ionization are comparable at both the N(1s) and O(1s) edges. Jaeger et. al. showed that XESD is the dominant indirect mechanism in H^+ desorption from thick NH_3 multilayers. Using gas-phase photon and electron absorption cross sections, we showed that N(1s) ionization by O(KLL) Auger electrons is a minor channel in XESD. We showed that ESD cross sections must be high ($>10^{-19}$ cm^2), but not unreasonably high, for valence shell XESD to be important. Furthermore, electron impact ionization cross sections are similar for many gases,[20] so that the discussion for the N_2-O_2 mixtures can be extended to many other condensed gases.

The most important, but unresolved, question is the extent to which XESD contributes to desorption from other materials. The claim is made[3,4] that XESD should be less important from ionic materials. However, ESD absolute thresholds at 10-40 eV are similar from most materials and ion yields increase monotonically in many materials until at least 100 eV electron kinetic energy. To determine when XESD is important one must know ESD absolute cross sections and electron energy distributions as functions of electron kinetic energy. Unfortunately, they are seldom reported in absolute units. ESD cross sections can vary widely: between 10^{-18} and 10^{-23} cm^2. XESD is probably important when the cross sections are high at 10^{-20} to

10^{-18} cm^2. Drinkwine and Lichtman[14] classified relative ESD cross sections into three shapes of curves as functions of electron kinetic energy. While the implications are concerning the XESD mechanism are unclear, the differences among these three shapes may be significant: the first shape resembles the characteristic electron absorption cross sections of Fig. 2 (or alternately, the inverse of the universal electron escape depth curve[21]), while the other two shapes are distinct.

Therefore, little is known about the contribution of XESD from materials in general. A large role of XESD has been established so far only in condensed multilayers. XESD is negligible in saturation coverages of CO on Ni(100) -- no structure in O^+ desorption is seen at the Ni(2p) threshold.[24] XESD was shown to be of minor importance in CO/W(100) in one of the earliest PSD experiments.[25] In many systems ion yield spectra differ from total electron yield, indicating that localized desorption mechanisms play a substantial role. In systems in which ion and electron yields are identical, no conclusions about the extent of XESD can be made. Determining materials in which XESD is unimportant is probably the most urgent problem in the ion desorption field.

Appendix

The role of XESD should be resolved by determining the factors in Eq. 1, in particular $\sigma_A(\epsilon)$ and $D(h\nu,\epsilon)$. A recent review article on secondary electron emission is of interest.[26] Use of an angle-resolved analyzer in estimating $D(h\nu,\epsilon)$ is unreliable for a variety of reasons. A simple, but well chosen, experiment could be helpful in understanding the role of XESD: the best technique for estimating $D(h\nu,\epsilon)$ is to bias the sample positively and measure the restoring current to the sample. One measures the current of all electrons emitted from the sample with greater than a cuttoff energy and within a wide range of angles. Using a series of batteries or a stable power supply, the sample bias can be scanned. One differentiates the resulting spectrum to obtain the distribution of electrons leaving the surface. While some electrons arriving at the surface are reflected, this distribution may be a good estimate of $D(h\nu,\epsilon)$. This simple experiment should be performed on a well-characterized sample, with known photon flux and known photoabsorption cross sections. Several ESD analyzers exist in which electron energy can be scanned, and presumably in which absolute ESD cross sections could be obtained. These experimental ESD cross sections are the upper bound on the term $\sigma_A(\epsilon)$ in Eq. 1 (an upper bound, because the experimental ESD cross sections have indirect channels of desorption folded in). With such a careful measurement, the terms $\sigma_A(\epsilon)$ and $D(h\nu,\epsilon)$ of Eq. 1 can be estimated, and the role of indirect mechanisms in stimulated desorption would be determined unambiguously.

Acknowledgements

This work was supported by the Director, Office of Energy Research, Office of Basic Energy Sciences, Chemical Sciences Division of the U. S. Department of Energy under Contract No. DE-AC03-76SF00098 and by the Naval Weapons Center Independent Research Fund, the Office of Naval Research. It was performed at the Stanford Synchrotron Radiation Laboratory, which is supported by the Department of Energy, Office of Basic Energy Sciences and the National Science Foundation, Division of Materials Research.

REFERENCES

*An abbreviated version of this discussion will be submitted to Phys. Rev. B with coauthors R. A. Rosenberg, P. J. Love, P. R. LaRoe, and V. Rehn.

1. P. J. Feibelman and M. L. Knotek, Phys. Rev. B 18, 6531 (1978).
2. M. L. Knotek, V. O. Jones, and V. Rehn, Phys. Rev. Lett. 43, 300 (1979).
3. R. Jaeger, J. Stöhr, and T. Kendelewicz, Phys. Rev. B 28, 1145 (1983).
4. R. Jaeger, J. Stöhr, and T. Kendelewicz, to be published.
5. R. A. Rosenberg, V. Rehn, A. K. Green, V. O. Jones, C. C. Parks, G. Loubriel, and R. H. Stulen, Chem. Phys. Lett. 80, 488 (1981).
6. R. A. Rosenberg, V. Rehn, A. K. Green, P. R. LaRoe, and C. C. Parks, in Proceedings of the First International Workshop on Desorption Induced by Electronic Transitions (DIET-1) (Williamsburg, Virginia, 1982), edited by N. H. Tolk, M. M. Traum, J. C. Tully, and T. E. Madey (Springer-Verlag, Berlin, 1983), page 247.
7. D. Charleston, Stanford Synchrotron Radiation Laboratory, private communication, July 1983.
8. C. C. Parks, Ph.D. Thesis, University of California - Berkeley 1983 (unpublished).
9. R. A. Rosenberg, P. J. Love, P. R. LaRoe, V. Rehn, and C. C. Parks, to be submitted to Phys. Rev. B.
10. A. P. Hitchcock and C. E. Brion, J. Electron Specr. Rel. Phenom.

18, 1 (1980).

11. E. Bauer, in Proceedings of the First International Workshop on Desorption Induced by Electronic Transitions (DIET-1) (Williamsburg, Virginia, 1982), edited by N. H. Tolk, M. M. Traum, J. C. Tully, and T. E. Madey (Springer-Verlag, Berlin, 1983), page 104.
12. M. L. Knotek, ibid., p139.
13. D. Menzel, J. Vac. Sci. Technol. 20, 538 (1982).
14. M. J. Drinkwine and D. Lichtman, Progress in Surf. Sci. 8 123 (1977).
15. R. E. LaVilla, J. Chem. Phys. 63, 2733 (1975).
16. S. Bodeur, C. Senemaud, and C. Bonnelle, Proceedings of the IV International Conference on Vacuum Ultraviolet Radiation Physics (Hamburg, 1974), edited by E. Koch, R. Haensel, and C. Kunz (Pergamon and Vieweg, Braunschweig, 1974), p94.
17. D. M. Barrus, R. L. Blake, A. J. Burek, K. C. Chambers, and A. L. Pregenzer, Phys. Rev. A 20, 1045 (1979).
18. G. Glupe and W. Mehlhorn, Phys. Lett. 25A, 274 (1967).
19. G. Ertl and J. Küppers, Low Energy Electrons and Surface Chemistry (Verlag Chemie, Weinheim, 1974).
20. L. J. Kieffer, Atomic Data 1, 19 (1969).
21. I. Lindau and W. E. Spicer, in Synchrotron Radiation Research, edited by H. Winick and S. Doniach (Plenum Press, N.Y., 1980), page 159.
22. T. E. Madey and J. T. Yates, J. Vac. Sci. Tech. 8 525 (1971).

23. R. Gomer, in Proceedings of the First International Workshop on Desorption Induced by Electronic Transitions (DIET-1) (Williamsburg, Virginia, 1982), edited by N. H. Tolk, M. M. Traum, J. C. Tully, and T. E. Madey (Springer-Verlag, Berlin, 1983), page 40.

24. R. Jaeger, R. Treichler, and J. Stöhr, Surf. Sci. 117, 533 (1982).

25. R. Franchy and D. Menzel, Phys. Rev. Lett. 43, 865 (1979).

26. For an extensive review: H. Seiler, in Secondary Electron Emission, submitted to Scanning Electron Microscopy, edited by R. M. Albrecht, J. D. Shelburne, and J. D. Meakin, (SEM, Inc., AMF O'Haire, Illinois).

27. H. Petersen, A. Bianconi, F. C. Brown, and R. Z. Bachrach, Chem. Phys. Lett. 58, 263 (1978).

TABLE I Differential increases of yields at the N(1s) and O(1s) edges for a N_2-O_2 mixture (N_2:O_2 ~ 1.35:1).

ION	EDGE	hν(eV)	IONS PER SEC[a]	IONS PER PHOTON[b]	IONS PER SURFACE IONIZATION[c]
N^+	N(1s)	420	348	2.5×10^{-6}	1.1×10^{-3}
O^+	N(1s)	420	26	1.9×10^{-7}	8.1×10^{-5}
N^+	O(1s)	540	61	8.5×10^{-7}	1.6×10^{-3}
O^+	O(1s)	540	24	3.3×10^{-7}	6.6×10^{-4}

a Assuming, for consistency with the literature, unity detection efficiency. Based on microchannel plate efficiencies to ions, an upper bound on detector efficiency is on the order of 20 percent.

b Based on a measured flux using a calibrated NBS photodiode at beam line III-1 of 10^7 photons/mA s at 420 eV and 30 μm slits (Ref. 7,8).

c Using photoabsorption cross sections of 2.3×10^{-18} cm^2 (Ref. 27) and 0.5×10^{-18} cm^2 (Ref. 15,16) for N_2 at 420 eV and O_2 at 540 eV, respectively. Ref. 17 gives 2.1×10^{-18} cm^2 as the cross section of O_2 at 540 eV. Throughout the manuscript, a coverage per atomic layer of 10^{15} molecules per cm^2 is used in calculations.

FIGURES

Fig.1 N^+, O^+, and total electron yield (TEY) from a condensed mixture of nitrogen and oxygen between the N(1s) and O(1s) photoabsorption thresholds.

Fig. 2 N_2 and O_2 gas phase ionization cross sections by electron bombardment as reported in Ref. 20. The error bars indicate the range of different measurements.

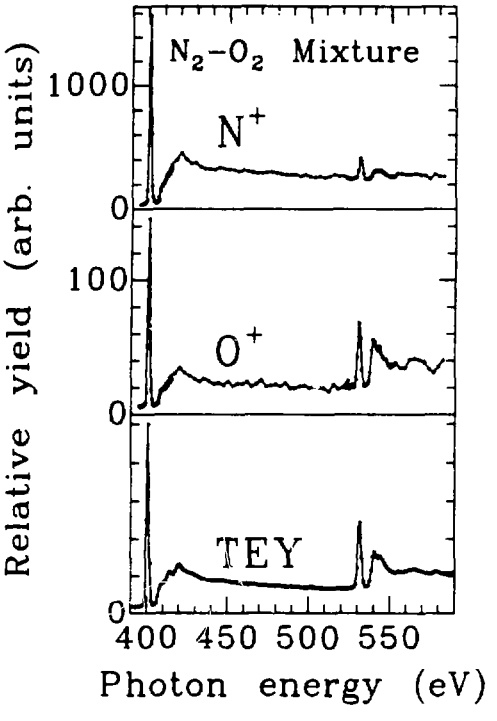

XBL 8310-11923

Figure 1

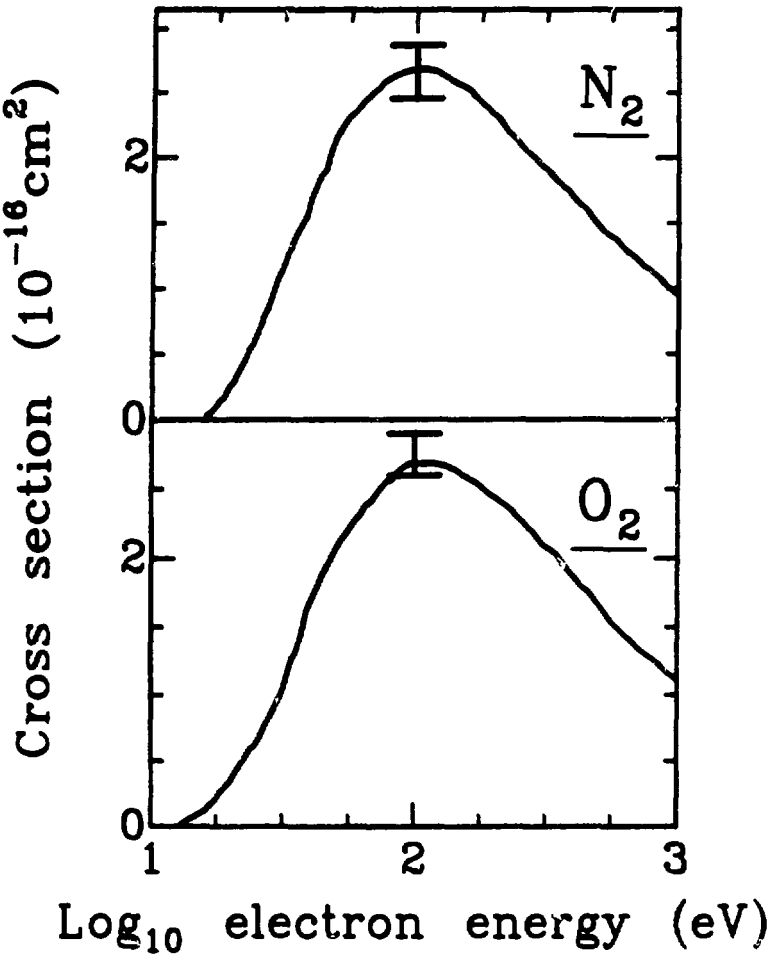

XBL 8310-11924

Figure 2

VI. PHOTON-STIMULATED DESORPTION FROM SOME ALKALI AND ALKALINE EARTH HALIDES

ABSTRACT

Results of photon-stimulated desorption measurements from several alkali halides and alkaline earth halides are reported. Ion desorption yields of KF at the K(2p) and K(1s) edges, CaF_2 at the Ca(2p) edge, and BaF_2 at the Ba(4d) edge are found to be roughly similar to photoabsorption spectra. The energetics of ion desorption from alkaline earth halides is found to be exothermic for halogen and alkaline earth positive ions, although experimentally Ba^{2+} is not observed. Ion yields from a series of alkali halides exhibit large variations in yields which cannot be explained by photoabsorption cross sections or by a model of two hole lifetimes.

A. Introduction

In this Chapter results are presented of photon-stimulated desorption (PSD) measurements from a series of alkali halides and alkaline earth halides. Three topics concerning the Auger decay model of desorption[1,2] are discussed. First, the Auger decay model predicts a rough correspondence of ion yield and bulk photoabsorption spectra. We compared PSD and photoabsorption spectra from KF, CaF_2, and BaF_2 at various photoabsorption thresholds and confirmed this rough correspondence. Second, we show that desorption of Ba^{2+} is exothermic in the Auger decay mechanism, yet we detected no Ba^{2+} in our mass spectra. Finally, the ion yields from a series of cleaved alkali halide crystals were compared. Two factors influencing ion desorption efficiency — the photoabsorption cross sections and the hole-hole lifetimes as estimated in the model of Cini[3] and Sawatzky,[4] -- are insufficient to understand the large variations in the ion yields.

B. Experimental

The experiments on CaF_2, BaF_2, and the $K(L_{2,3})$ edge of KF were performed on Beam Line III-1 at the Stanford Synchrotron Radiation Laboratory, using a "grasshopper" monochromator equipped with 600 and 1200 line/mm gratings. The experiment on the K(1s) edge of KF was performed at Beam Line III-3, using a double crystal monochromator with Ge(111) monochromator crystals. Charging was minimized by coating the sides of the samples with graphite before insertion in the vacuum chamber. While in the K(1s) experiment no precautions were taken, in the $K(L_{2,3})$ edge experiment the hydroscopic KF sample was mounted onto the sample plate in a nitrogen-filled glove bag to minimize contact with moisture. Optical quality single crystals were cleaved *in situ* along the (001) plane of KF and the (111) plane of CaF_2 and BaF_2 at a pressure of 10^{-9} torr. The positive ion yields were collected using a time-of-flight analyzer. The ion- and prompt- yield spectra were normalized to the incident photon flux as measured by the electron yield from a graphite-coated grid.

C. Results and Discussion

In this section, ion yield spectra versus photon energy, ion yields and energetics of ion desorption from BaF_2, and ion yields from some alkali halides are discussed separately.

1. Ion Yield Spectra Versus Photon Energy of KF, CaF_2, and BaF_2

A major test of the Auger decay mechanism is to compare ion yield spectra to photoabsorption spectra near photoabsorption thresholds. A close correspondence of ion yields to photoabsorption was expected and obtained in PSD from NaF near the Na(1s) edge.[5] In PSD near the Li(1s) and F(2s) edges in LiF, the Li^+ yield had no threshold near the F(2s) edge, contrary to expectation.[6] Therefore it is of interest to compare ion yields to photoabsorption from other systems. Our purpose in this section is to demonstrate a rough correspondence of PSD to bulk photoabsorption from KF and CaF_2 at the $K^+(2p)$ and $Ca^{2+}(2p)$ edges, from KF at the $K^+(1s)$ edge, and from BaF_2 at the $Ba^{2+}(4d)$ threshold.

The photoabsorption and PSD spectra near the metal $L_{2,3}$ edges of CaF_2 and KF are presented first. The photoabsorption spectrum[7,8] of CaF_2 in the lower panel of Fig. 1 exhibits features common to many K^+ and Ca^{2+} compounds. The spin-orbit split peaks B and D, occuring about 3.5 eV below the respective photoionization thresholds,[7] were assigned to the $Ca^{2+}(2p \rightarrow 3d)$ excitons, and peaks A and C were assigned to splitting of the 3d states in the crystal field. The PSD spectrum is compared to the broadened photoabsorption

spectrum in the upper panel of Fig. 1. The photoabsorption spectrum was broadened with a Gaussian function to match the 2.0 eV monochromator resolution of the PSD spectrum. The PSD and photoabsorption spectra agree roughly: in particular both ion yields and photoabsorption increase below the photoionization threshold. In more detail, the PSD spectra are sharper than the broadened photoabsorption spectra, more than can be explained by uncertainty in monochromator resolution. We suggest that the the crystal-field peaks A and B, which are sensitive to chemical environment, are partially suppressed in the PSD spectrum. The photoabsorption spectrum[8] near the $K(L_{2,3})$ edge of KF, shown in the lower panel of Fig. 2, also exhibits the 3d exciton peaks B and D below the photoionization threshold and the much larger crystal field peaks A and C. The PSD spectrum of impurity H^+ is in qualitative agreement with the broadened photoabsorption spectrum and the total electron yield.

A comparison of the ion yield, electron yield, and photoabsorption[9] spectra from KF at the K(1s) edge is shown in Fig. 3. The photoabsorption spectrum of KF has not been interpreted previously. In KCl, the conduction band minimum [3610.7 eV (Refs. 10,11)] lies near[12] the first peak in photoabsorption [3426.9 XU (Ref. 9) or 3610.4 eV], contrary to early work[13,14] which assigned the first peak to a core exciton. In comparing the series of potassium halides, the K(1s) edges agree closely,[9] but the structures above threshold vary considerably. The spacing between the first two peaks is particularily wide (8.4 eV) in KF. The PSD spectra in Fig. 3 from KF

are in qualitative agreement with the photoabsorption and the total electron yield spectra. The apparent smaller magnitude of the first peak in the F^+ spectrum in Fig. 2 was not reproducible.

Next we consider PSD and photoabsorption of BaF_2 at the Ba(4d) threshold. The ionicity of BaF_2 is probably very high because of the close agreement of the theoretical cohesion energy of the Born model and the experimental cohesion energy.[15] Therefore, it is of interest to compare photoabsorption spectra of BaF_2 to that of Ba^{2+} vapor. This comparison has been made previously[16-18] and is reproduced in Fig. 4. The Ba^{2+} spectrum, even when broadened to simulate possible effects of condensation, agrees poorly with the BaF_2 spectrum, although features A, B, and D might be related to some of the gas phase features. Feature D is shifted in the other barium halides,[17] as a further indication of the failures of the atomic approach in these complex salts. The electron yield of Hecht[18,19] and H^+ PSD spectra are compared in Fig. 5. Some of the differences between the two spectra are artifacts. For instance, the small peaks near 90 and 106 eV cannot be seen in the PSD spectra because of poorer monochromator resolution, and the relative heights of peaks B and D are different in part because of differences in normalization. Some electron yield spectra that I took are in better agreement with the PSD, but are not shown here because the spectrum of Hecht is generally of better quality. Therefore, as in the other systems, the PSD is in qualitative agreement with photoabsorption.

2. Ion Yields and Energetics of Desorption from BaF_2

The first PSD ion yield mass spectra from a compound of fluorite structure are reported. The major desorbing species from cleaved BaF_2 were F^+ and impurity H^+ and OH^+. No Ba^{2+} yield was detected. It is shown that desorption of Ba^{2+} and F^+ is favorable energetically in the Auger decay model, and that other factors must be examined to understand the lack of Ba^{2+} yield.

Two ion yield spectra from BaF_2, acquired 15 and 90 minutes after sample cleavage, are displayed in Fig. 6. While the spectra were taken with different photon energies, we believe that the growth of H^+ and OH^+ yields with time was real. A possible source of the OH^+ yield was adsorbed water. Both spectra lack ion species other than H^+, OH^+ and F^+. Using Eqs. 1-6 of Chap. II and the F^+ time-of-flight we estimate that Ba^{2+} should appear at about 500 ns and that the width of the peak should be comparable (within a factor of two) with that of F^+. Thus the Ba^{2+} yield was less than a few percent that of F^+.

The energetics of ion desorption in PSD from alkali halides was developed in Chap. III using the Born model of cohesion of ionic solids and the polarization model of Mott and Littleton. It was shown that production of a positive halogen ion X^+ in an Auger decay cascade was crucial in the desorption of positive ions. The net environments of the X^+ ion and the surrounding metal ions M^+ were shown to be repulsive, as is required for desorption to occur. The

same analysis is applied to BaF_2. Use of the Born model for BaF_2 is justified by the close agreement (0.5 percent) of the cohesive energy as estimated by the Born model and as measured using the Born-Haber cycle.[15]

The equations in Chap. III for the maximal energy available to a desorbing ion must be generalized slightly to include compounds of formula $M^{n+}X_n^-$. Following Chap. III, we consider the M^{n+} ion desorbing from an ionic lattice, in which z electrons have been removed from a neighboring halogen ion. The repulsion energy U^{n+} of the M^{n+} ion is

$$U^{n+} \sim \frac{n z e^2}{r k_{eff}} , \qquad (1)$$

where e is the electron charge, r is the distance between the M^{n+} ion and the halogen under consideration, and k_{eff} is the effective dielectric constant. The net energy E^{n+} for desorption of a M^{n+} ion is

$$E^{n+} = U^{n+} - \alpha E_M^{n+} + \beta E_{BR}^{n+} + \gamma\, 0.5\, e\, \phi^{n+} , \qquad (2)$$

where E_M^{n+}, E_{BR}^{n+}, and ϕ^{n+} are the bulk Madelung energy, Born repulsion energy, and polarization potential, respectively, of the M^{n+} ion. α, β, and γ are the corresponding surface correction terms (with values between one and zero).

Let us evaluate the desorption energetics of BaF_2. While the

partitioning of the Madelung energy into its positive and negative ion components is nontrivial in general, E_M^{2+} was determined to be 17.59 eV for BaF_2 (using symmetry and the fact that the fluorite structure is a superposition of the CsCl and NaCl lattices).[20] E_{BR}^{2+} was determined previously[20] to be 3.88 eV. The polarization for the rigidly-held lattice[20] is 2.02 eV; the polarization correction in Eq. 2 is somewhat larger because the lattice can relax partially. The nearest neighbor F^-——Ba^{2+} distance[21] is 2.68 Å, so that $U^{2+} = 10.74\ z$ eV. To obtain rough estimates of E^{2+}, we set $k_{eff} = \alpha = \beta = \gamma = 1$. E^{2+} is slightly endothermic for z=1, indicating that Ba^{2+} cannot desorb from majority sites following single ionization of halogen. For production of a positive halogen ion (z=2) we obtain $E^{2+} \sim 9.8$ eV, clearly sufficient to expel a Ba^{2+} ion from the surface.

The energy E^- available to a desorbing positive halogen ion is

$$E^- = \alpha E_M^- + \beta E_{BR}^- - \gamma\ 0.5\ e\ \phi^- \ . \qquad (3)$$

The Madelung energy E_M^- is 9.45 eV for BaF_2 (Ref. 20). The Born repulsion term E_{BR}^- and the polarization term of the F^+ ion, while nontrivial to estimate, are no more than two or three electron volts in magnitude. Therefore, it is also energetically possible for F^+ to desorb.

In summary, the major desorbing species from a cleaved BaF_2 surface are F^+ and impurity H^+ and OH^+. Ba^{2+} did not desorb,

yet the energetics of desorption for both Ba^{2+} and F^+ are favorable.

3. Ion Yields from some Alkali Halides

Preliminary data on wide variations of ion yields from a series of alkali halides are presented here. Some of the factors influencing desorption probabilities — photoabsorption cross sections and two hole lifetimes of excited halogen ions — are insufficient to explain the experimental trends. The role of other factors — the probability that decay of the core hole will produce a localized two hole state, and the dependence of ion yields on "extraneous" factors such as surface roughness, impurities, and defect concentrations — must be considered.

Ion yields from a series of alkali halides are displayed in Table I. Yields were obtained in a single experiment to minimize systematic error. These results are tentative because reproducibility of yields with sample cleavage was tested only once for NaCl and NaF. We observe the following trends: yields from the fluorides exceed (by a factor of 8 to 40) yields from the chlorides. Yields from sodium halides also exceed (by a factor of 3 to 12) yields from potassium halides. Alkali ion yields are greater than halogen yields. The H^+ yields (which grow with beam exposure in these systems) from the fluorides are greater than those from the chlorides.

We can predict trends in ion yields within the Auger decay model. The ion yields from the alkali halides depend on 1) the photoabsorption cross sections of the alkali metal np and ns and halogen ns levels, 2) the probability that the core hole decays to produce a positive halogen X^+, 3) the lifetime of the two hole X^+ state, and 4) a characteristic time (~ 10^{-12} s) that the desorbing ion takes to escape from the lattice. We can estimate the effects of factors 1), 3) and 4), but factor 2) is beyond the scope of this study.

Photoabsorption cross sections do not account for the yield variations. For example, we compare NaF (isoelectronic with Ne) and KCl (isoelectronic with Ar). The calculated Ne subshell ns and np photoionization cross sections[22] are greater than those of Ar by only a factor of two at $h\nu$ = 151 eV. The ratio (about 100) between ion yields from NaF and ion yields from KCl is much too large to be explained by differences in photoabsorption cross sections of the respective ions.[23]

The relative lifetimes of the halogen ions X^+ can be estimated using a model of Cini[3] and Sawatzky.[4] When the two hole Coulomb repulsion U is greater than the valence band width 2Δ, the holes become bound, resulting in an enhanced lifetime and enhanced ion yield.[24,25] The "two hole" Coulomb repulsion is the difference in energy of the X^+ ion and neutral X^0 in the crystal. In a Born-Haber cycle, U is roughly the sum of the Madelung energy[26] of the X^- ion and the halogen ionization potential. Using U and the experimental valence band widths,[26] we obtain the ratio $U:2\Delta$ equal

to 5.78, 7.25, 5.34, and 7.77 for NaF, KF, NaCl, and KCl, respectively. If we expected any trends at all on the basis of these rather similar ratios, we would predict the X^+ lifetimes and ion yields of the potassium halides to be greater. Contrary to this expectation, yields from NaF are greater than yields from KF; yields from NaCl exceed yields from KCl.

The final consideration is the characteristic time of desorption. If the ions desorb with comparable kinetic energies, the heavier ions take longer to desorb. If the characteristic time of desorption is comparable to the two hole lifetime, the lighter masses are favored to desorb. Consistent with this idea, yields of the heavier Cl^+ and K^+ ions are less than yields of the F^+ and Na^+ ions. This concept explains only some of the results in Table I, but not, for instance, the higher yield of Na^+ from NaF versus NaCl.

In summary, ion yields from the alkali halides vary widely. In general the fluorides have higher alkali, halogen, and hydrogen ion yields than the chlorides. Sodium halides have higher yields than potassium halides. These trends cannot be understood in terms of photoabsorption cross section or in terms of the hole-hole lifetime model of Cini and Sawatsky and other factors must be considered.

D. Summary

Results of PSD measurements from several alkali halides and alkaline earth halides were presented. Three topics concerning the Auger decay mechanism were discussed. First, a rough correspondence of bulk photoabsorption and PSD yields from various core thresholds of KF, CaF_2 and BaF_2 was demonstrated. This correspondence is in agreement with the expectations of the Auger decay mechanism. Second, the energetics of ion desorption from BaF_2 was found to be favorable for both Ba^{2+} and F^+ ions, while experimentally no desorption of Ba^{2+} was found. Finally, relative ion yields from a series of alkali halides were presented. While many factors influence ion yields, it was found that the results could not be explained in terms of photoabsorption cross sections or in terms of a model of hole-hole lifetimes.

Acknowledgments

I would like to thank R. Stulen, G. Loubriel, and M. L. Knotek of Sandia National Laboratories for the use of their sample chamber and M. L. Knotek in particular for help in preparing the experiments. This work was supported by the Director, Office of Energy Research, Office of Basic Energy Sciences, Chemical Sciences Division of the U. S. Department of Energy under Contract No. DE-AC03-76SF00098. It was performed at the Stanford Synchrotron Radiation Laboratory, which is supported by the Department of Energy, Office of Basic Energy Sciences and the National Science Foundation, Division of Materials Research.

REFERENCES

*This chapter is based in part on experiments performed in collaboration with R. Rosenberg, P. LaRoe, P. Love, V. Rehn, and D. A. Shirley.

1. P. J. Feibelman and M. L. Knotek, Phys. Rev. B 18, 6531 (1978).

2. M. L. Knotek, V. O. Jones, and V. Rehn, Phys. Rev. Lett. 43, 300 (1979).

3. M. Cini, Solid State Commun. 24, 681 (1977).

4. G. A. Sawatzky, Phys. Rev. Lett. 39, 504 (1977).

5. C. C. Parks, Z. Hussain, D. A. Shirley, M. L. Knotek, G. Loubriel, and R. A. Rosenberg, Phys. Rev. B 28, no. 8 (1983).

6. C. C. Parks, D. A. Shirley, and G. Loubriel, submitted to Phys. Rev. B.

7. R. E. Ruus, A. A. Maiste, and Yu. A. Maksimov, Izvestiya Akademii Nauk SSSR, Seriya Fizicheskaya 46, 789 (1982).

8. A. A. Maiste, R. E. Ruus, and M. A. Elango, Zh. Eksp. Teor. Fiz. 79, 1671 (1980).

9. C. Sugiura, Science Reports of the Tohoku University, First Series 45, 249 (1961).

10. L. N. Mazalov, E. E. Vainshtein, and V. G. Zyryanov, Doklady Akademii Nauk SSSR 164, 545 (1965).

11. The K(1s) to conduction band transition energy of KCl is reported as 3611 eV by Kai Siegbahn, C. Nordling, A. Fahlman, et. al. in Electron Spectroscopy for Chemical Analysis (National Technical Information Service, Springfield VA 1968), p66.

12. L. N. Mazalov, S. M. Blokhin, and E. E. Vainshtein, Fizika

Tverdogo Tela 8, 2420 (1966).

13. L. G. Parratt and E. L. Jossem, Phys. Rev. 97, 916 (1955).

14. L. G. Parratt and E. L. Jossem, J. Phys. Chem. Solids 2, 67 (1957). The estimated position of the conduction band in KCl is too high if the presently accepted valence band width (2.7 eV FWHM in Ref. 27) is used.

15. J. Sherman, Chem. Rev. 11, 93 (1932).

16. T. B. Lucatorto, T. J. McIlrath, J. Sugar, and S. M. Younger, Phys. Rev. Lett. 47, 1124 (1981).

17. T. B. Lucatorto, T. J. McIlrath, W. T. Hill III, and C. W. Clark, in X-Ray and Atomic Inner-Shell Physics-1982, edited by B. Crasemann, (American Institute of Physics, New York, 1982), p584.

18. M. H. Hecht, Ph. D. Thesis, Stanford University, 1982, (unpublished).

19. M. H. Hecht and I. Lindau, Stanford Synchrotron Radiation Laboratory Activity Report 4/1/81-3/31/82, edited by A. Bienenstock and H. Winick, May 1982 (unpublished).

20. R. T. Poole, J. Szajman, R. C. G. Leckey, J. G. Jenkin, and J. Liesegang, Phys. Rev. B 12, 5872 (1975).

21. L. Pauling, The Nature of the Chemical Bond, 3d edition, (Cornell University Press, Ithaca, 1960).

22. I. M. Band, Yu. I. Kharitonov, and M. B. Trzhaskovskaya, Atomic Data and Nuclear Data Tables 23, 443 (1979).

23. Some work on relative peak intensities in photoelectron spectroscopy from alkali halides is relevant. See T. Ohta, S.

Kinoshita, and H. Kuroda, J. Electron Spectr. Relat. Phenom. 12, 169 (1977); K. T. Ng and D. M. Hercules, J. Electron Spectr. Relat. Phenom. 7, 257 (1975); T. Sugano, M. Sakairi, M. Yamada, N. Kosugi, H. Kuroda, H. Daimon, Y. Murata, in Activity Report of the Synchrotron Radiation Laboratory—1979, Institute for Solid State Physics (University of Tokyo, Tokyo, 1980), unpublished, page 67.

24. D. E. Ramaker, C. T. White, and J. S. Murday, J. Vac. Sci. Technol. 18, 748 (1981).

25. P. J. Feibelman, Surf. Sci. 102, L51 (1981).

26. M. P. Tosi in Cohesion of Ionic Solids in the Born Model, Vol. 16 of Solid State Physics, edited by F. Seitz and D. Turnbull (Academic Press, New York, 1964).

27. The experimental valence band widths are 4.9, 3.7, 4.1, and 2.7 eV FWHM for NaF, KF, NaCl, and KCl, respectively. R. T. Poole, J. G. Jenkin, J. Liesegang, and R. C. G. Leckey, Phys. Rev. B 11, 5179 (1975).

TABLE 1 Approximate relative PSD yields from some alkali halides at $h\nu \approx 160$ eV.

	LiF	NaF	NaCl	KF	KCl
CATION					
Li,Na,K	7–9	25–50	2.5–4.5	10–15	0.3
ANION					
F,Cl	2–3	12–30	0.6–1.0	1.5–2.0	0.2
H	10–17	22–110	0.8	50–60	1.0

FIGURE CAPTIONS

Fig. 1. Lower panel: the photoabsorption measurements (Ref. 7,8) at the Ca($L_{2,3}$) edge of CaF_2, performed at a resolution of 0.3–0.6 eV. An arrow marks the estimated (Ref. 7) L_3 to conduction band transition energy. Upper panel: F^+ PSD (large dots) compared to the broadened photoabsorption spectrum (solid line). The photoabsorption spectrum was broadened by a 1.86 eV Gaussian function to match the PSD monochromator resolution of 2 eV.

Fig. 2. Lower panel: the photoabsorption measurements (Ref. 8) at the K($L_{2,3}$) edge of KF, performed at a resolution of 0.2–0.6 eV. An arrow marks the position of the estimated (Ref. 8) L_3 to conduction band transition energy. Middle panel: total electron yield. Upper panel: H^+ PSD (large dots) compared to the broadened photoabsorption spectrum (solid line). The photoabsorption spectrum was broadened by a 1.86 eV Gaussian function to match the PSD monochromator resolution of 2 eV.

Fig. 3. Lower panel: the photoabsorption measurements (Ref. 9) at the K(K) edge of KF. Other panels: H^+, F^+, K^+ and electron yields from KF, performed with a photon energy resolution of about 1.7 eV.

Fig. 4. Photoabsorption spectra of Ba and Ba^{2+} vapor (Ref. 16), spectra of Ba^{2+} vapor broadened by a 2 and a 3 eV Gaussian function, and the electron yield (Ref. 19) from BaF_2.

Fig. 5. Lower panel: total electron yield (Ref. 19) from BaF_2
Upper panel: H^+ PSD spectrum from BaF_2, conducted with a monochromator resolution of 0.8 eV at 120 eV.

Fig. 6. Upper panel: time-of-flight mass spectrum from a BaF_2 crystal 15 minutes after cleavage taken with zero order light. Lower panel: time of flight mass spectrum 90 minutes after cleavage at $h\nu$ = 100 eV.

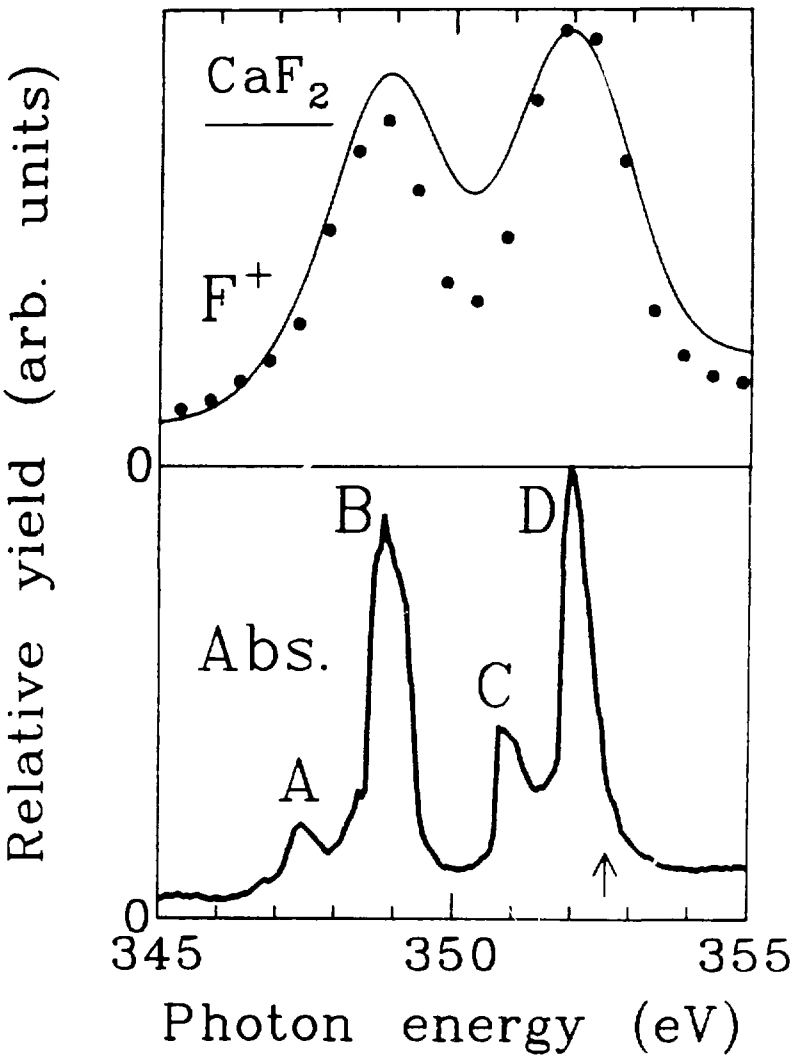

XBL 8310-11925

Figure 1

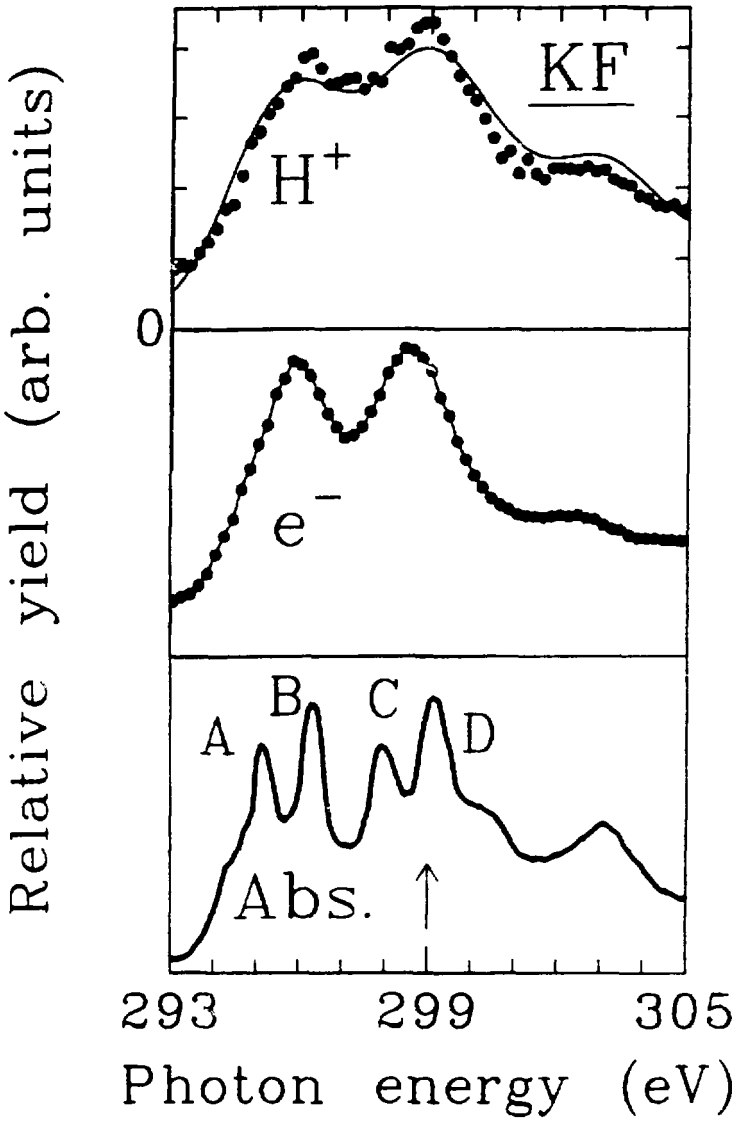

XBL 8310-11926

Figure 2

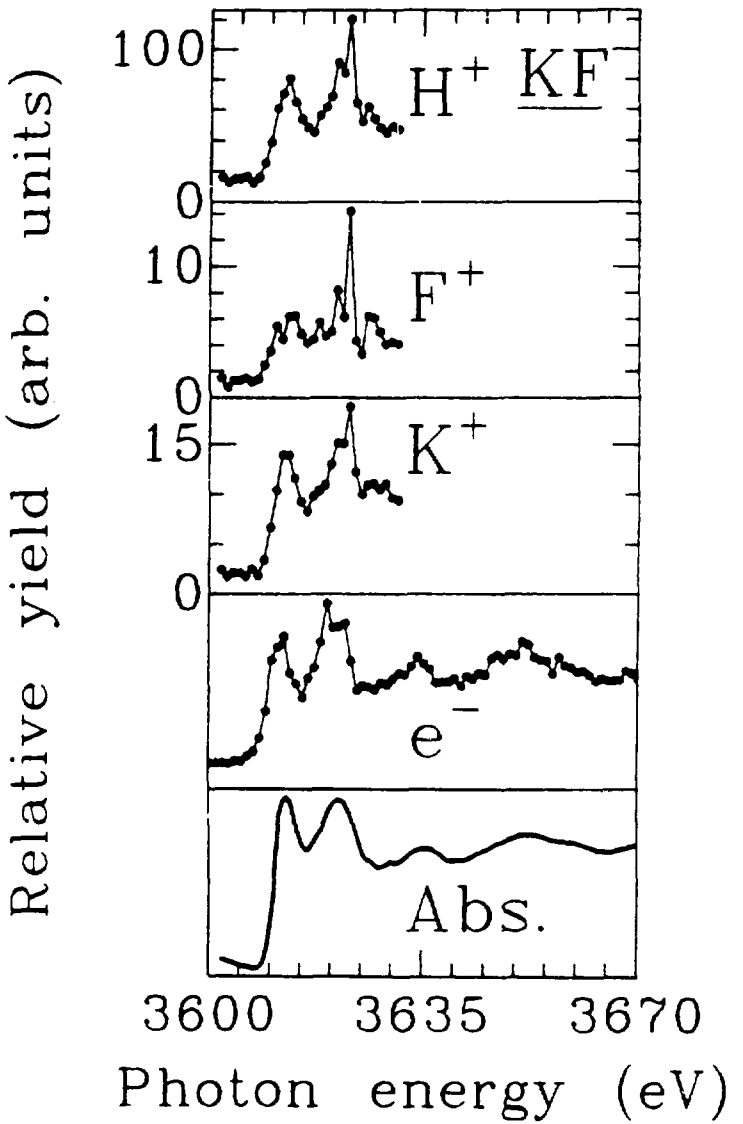

XBL 8310-11927

Figure 3

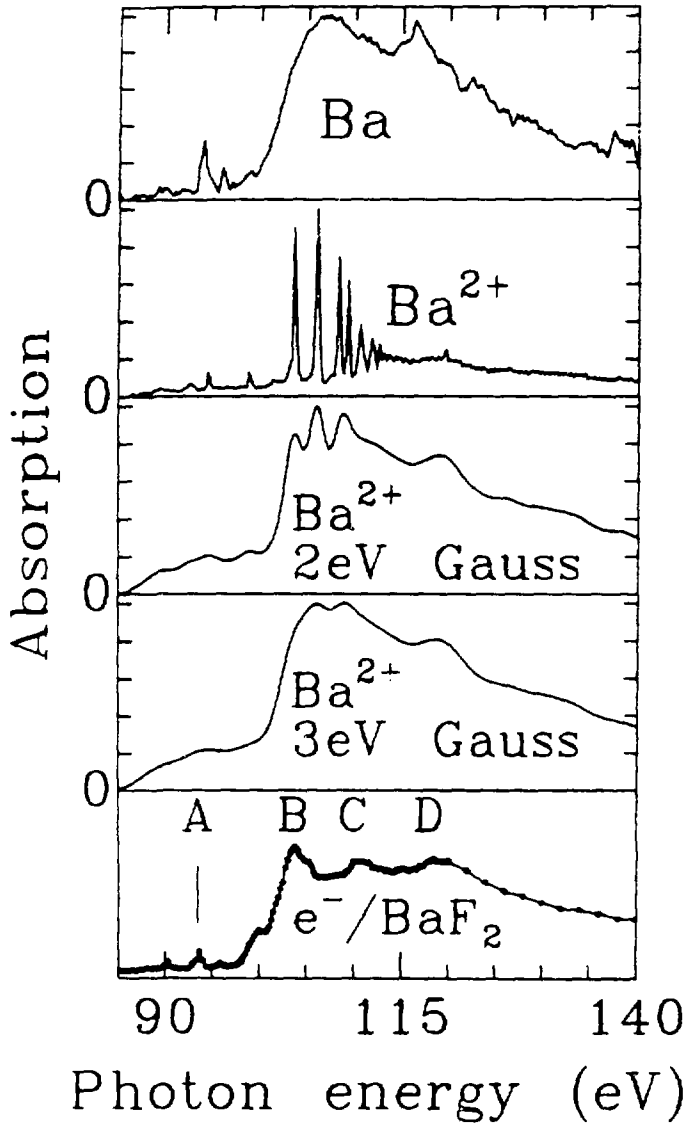

XBL 8310-11928

Figure 4

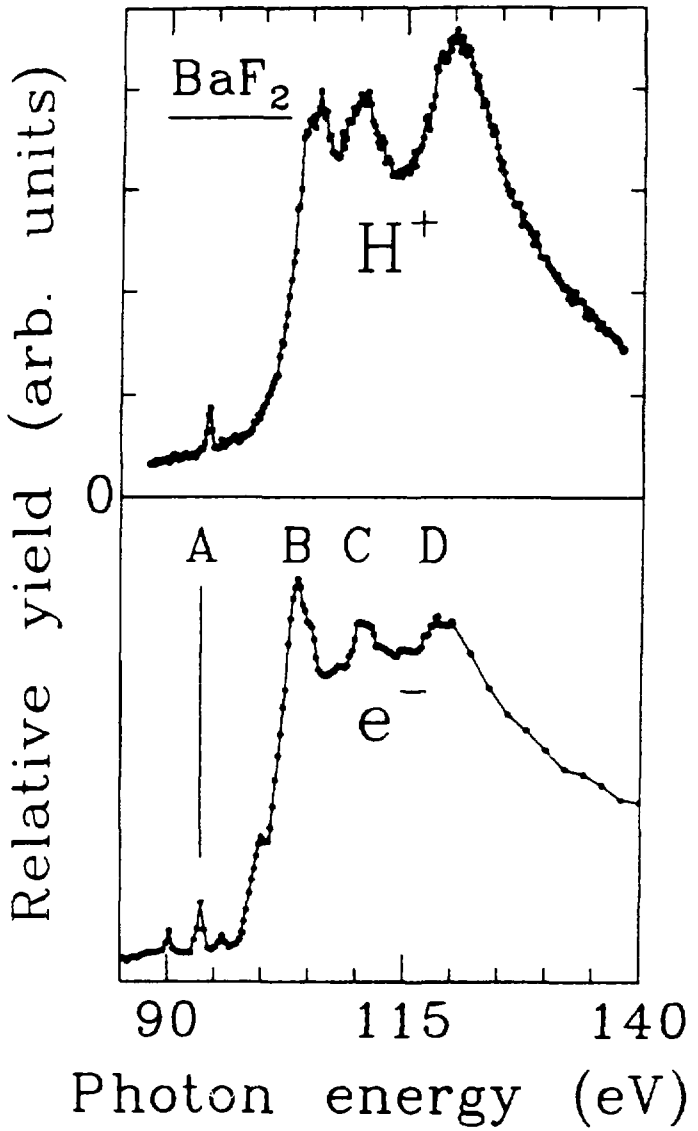

XBL 8310-11929

Figure 5

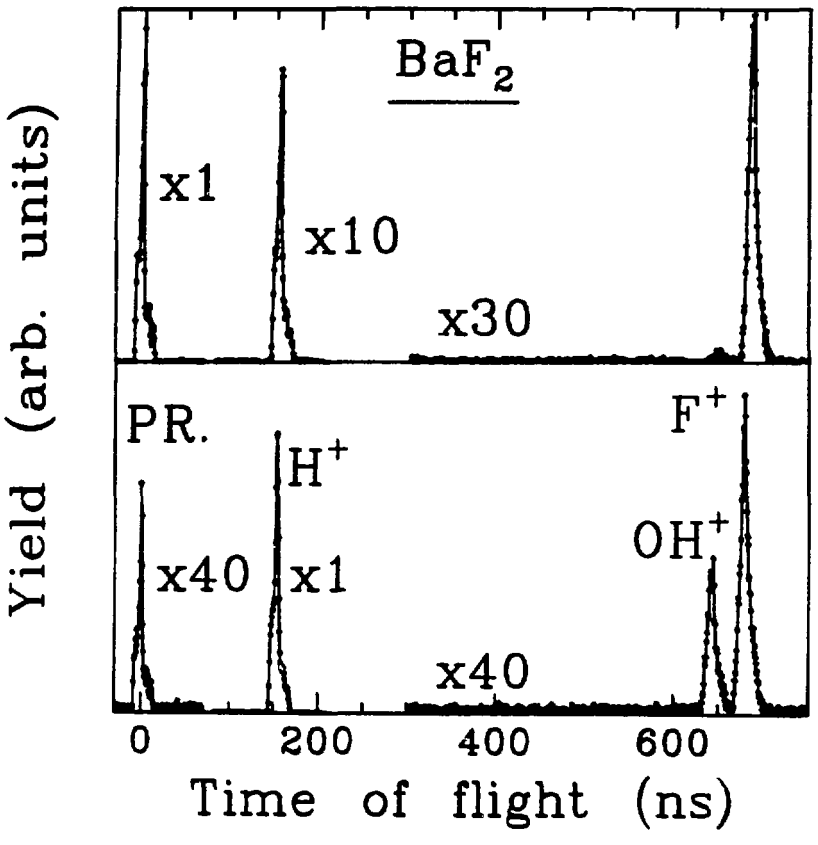

XBL 8310-12089

Figure 6

VII. CONCLUDING REMARKS

The final chapter of a doctoral thesis is perhaps the most valuable as an evaluation of a field of study. I have had the good fortune of performing many of the early experiments since photon-stimulated desorption (PSD) of positive ions was discovered in 1979. With this perspective I briefly assess what I call three periods of research in electron stimulated desorption (ESD) and PSD. The first (1942-1979) was a period of discovery of the basic phenomena and mechanisms. The second (1979-1983: my tenure as a graduate student) was a period of transition in which some concepts crystallized but some crucial difficulties were identified. In the future period some fundamental questions must be answered before the true potential of ESD and PSD can be evaluated.

A. The Past (1942-1979)

Results from this period are outlined in a series of review papers.[1-6] ESD was first studied systematically by Isikawa[7] in 1942. By 1975 the following experimental facts were known: ESD was proportional to electron current, the ESD thresholds for ions occurred between 15 and 40 eV, ESD yields were not proportional to coverage, only a small fraction (10^{-3} to 10^{-6}) of surface ionizations resulted in ion desorption, ion kinetic energies were between 0 and 10 eV, an isotope dependence of yields occured, and desorption

exhibited angular distributions which were related to bonding directions. The Menzel-Gomer-Redhead (MGR) model[8,9] was formulated (1964) to understand these results. This completely general mechanism[10] has two steps: a transition within the Franck-Condon approximation to a repulsive excited state and desorption in competition with delocalization of the excitation. Unfortunately, the generality of this mechanism obscured the essential nature of the repulsive states for many years. The next major development came in 1978 when Knotek and Feibelman discovered that ion yield thresholds correlated with core level thresholds[11,12] -- in spite of the substantially lower cross sections of core levels. This led to the formulation of the Auger decay mechanism, the sudden realization that PSD must occur, and the dramatic confirmation[13] of PSD at the Stanford Synchrotron Radiation Laboratory in 1979 by Knotek, Jones, and Rehn.

B. The Recent Past (1979-1983)

As the potential of PSD as a site-specific probe became apparent, many research groups jumped into the fray. Franchy and Menzel established in an early study (1979) that PSD occured by an intrinsic photoeffect[14] from a particular system [CO/W(100)]. Desorption thresholds corresponding to core levels were quickly confirmed from a wide variety of materials[15] - adsorbate systems, van der Waals solids, semiconductors, and insulators.

Inevitably a more complex picture emerged. Theoretically it became apparent that multihole repulsive states — *in* valence[16,17] and core[18-20] level absorption — dominated ion desorption, and that the simple Auger decay mechanism needed to be generalized. A model for understanding the long multihole lifetimes necessary for desorption to occur was adopted from earlier work of Cini[21] and Sawatzki.[22] A delayed onset of O^+ desorption from CO/Ni(100) at the O(1s) edge (Jaeger, Treichler, and Stöhr 1982) demonstrated a failure of the Auger decay mechanism and the need to consider multielectron excitations.[23] With this study came the recognition that the ultimate goal of PSD — to become an easily interpretable probe of surfaces — was elusive. The role of low intensity beam exposures in changing ion yields in certain materials (alkali fluorides[24,25] and possibly cleaved silicon[26]) demonstrated that PSD might become a unique probe of certain defect properties. The demonstration (Jaeger, Stöhr, and Kendelewicz 1983) that an indirect mechanism of desorption (x-ray induced ESD) predominated in ion desorption from condensed multilayers[27,28] shattered the assumption that ESD and PSD were inherently site-specific probes. Bonding-site specificity of PSD was demonstrated in other systems,[29] however, such as O^+ from Na_xWO_3 (Benbow, Thuler, and Hurych 1982). Angular distributions of ions from adsorbate systems proved to be important[30] (Madey et. al.) for adsorbate systems. Important experiments on stimulated desorption of neutrals (from alkali halides[31] — Tolk et. al. 1983; from adsorbate systems[32]— Menzel 1982) and negative ions[33,34] were also

performed.

C. The Future

The major challenge of the future is to determine the contribution of each of the three mechanisms -- X-ray induced ESD (XESD), the Auger decay mechanism, and the MGR mechanism. The usefulness of PSD and ESD in cases where XESD predominates is very limited, yet the extent that XESD contributes is largely unknown. So far a major role of XESD has been established only for condensed multilayers. When the Auger decay mechanism predominates, PSD is a unique and powerful probe of site-specific photoabsorption cross sections. Interpretations of cases in which the general MGR mechanism applies will require difficult calculations and progress will be limited to simple systems for many years to come. However, fundamental new insights into coupling of fast electronic decay processes to nuclear motion should emerge from these studies of the MGR mechanism. New electron-ion coincidence experiments are being planned which may yield direct information on ion desorption mechanisms.

REFERENCES

1. M. J. Drinkwine and D. Lichtman, Prog. Surf. Sci. 8, 123 (1977).
2. R. Gomer, Solid State Physics 30, 93 (1976).
3. D. Menzel, in Topics in Applied Physics, 4, edited by R. Gomer (Springer Verlag, Berlin, 1975).
4. D. Menzel, Surf. Sci. 47, 370 (1975).
5. T. E. Madey and J. T. Yates, J. Vac. Sci. Technol. 8, 525 (1971).
6. D. Menzel, Angew. Chem. Internat. Edit., 9, 255 (1970).
7. Y. Isikawa, Rev. Phys. Chem. Jap. 16, 83, 117 (1942).
8. P. A. Redhead, Can. J. Phys. 42, 886 (1964).
9. D. Menzel and R. Gomer, J. Chem. Phys. 41, 3311 (1964).
10. D. Menzel, in Desorption Induced by Electronic Transitions (DIET-1), edited by N. H. Tolk, M. M. Traum, J. C. Tully, and T. E. Madey, (Springer-Verlag, Berlin, 1983), p53.
11. M. L. Knotek and P. J. Feibelman, Phys. Rev. Lett. 40, 964 (1978).
12. P. J. Feibelman and M. L. Knotek, Phys. Rev. B 18, 6531 (1978).
13. M. L. Knotek, V. O. Jones, and V. Rehn, Phys. Rev. Lett. 43, 300 (1979).
14. R. Franchy and D. Menzel, Phys. Rev. Lett. 43, 865 (1979).
15. For a survey, see: Desorption Induced by Electronic Transitions (DIET-1), edited by N. H. Tolk, M. M. Traum, J. C. Tully, and T. E. Madey, (Springer-Verlag, Berlin, 1983).
16. C. F. Melius, J. O. Noell, and R. H. Stulen, J. Vac. Sci. Technol. 20, 559 (1982).
17. R. A. Rosenberg, V. Rehn, A. K. Green, P. R. LaRoe, and C. C.

Parks, Phys. Rev. Lett. 51, 915 (1983).

18. D. E. Ramaker, C. T. White, and J. S. Murday, Phys. Lett. 89A, 211 (1982).

19. D. E. Ramaker, C. T. White, and J. S. Murday, J. Vac. Sci. Technol. 18, 748 (1981).

20. P. J. Feibelman, Surf. Sci. 102, L51 (1981).

21. M. Cini, Solid State Commun. 24, 681 (1977).

22. G. A. Sawatzky, Phys. Rev. Lett. 39, 504 (1977).

23. R. Jaeger, J. Stöhr, R. Treichler, and K. Baberschke, Phys. Rev. Lett. 47, 1300 (1981).

24. C. C. Parks, Ph.D. Thesis, University of California - Berkeley, 1983 (unpublished).

25. C. C. Parks, D. A. Shirley, and G. Loubriel, submitted to Phys. Rev. B.

26. M. L. Knotek, G. M. Loubriel, R. H. Stulen, C. C. Parks, B. E. Koel, and Z. Hussain, Phys. Rev. B 26, 2292 (1982).

27. R. Jaeger, J. Stöhr, and T. Kendelewicz, Phys. Rev. B 28, 1145 (1983).

28. R. Jaeger, J. Stöhr, and T. Kendelewicz, unpublished.

29. R. L. Benbow, M. R. Thuler, and Z. Hurych, Phys. Rev. Lett. 49, 1264 (1982).

30. T. E. Madey, F. P. Netzer, J. E. Houston, D. M. Hanson, and R. Stockbauer, in Desorption Induced by Electronic Transitions (DIET-1), edited by N. H. Tolk, M. M. Traum, J. C. Tully, and T. E. Madey, (Springer-Verlag, Berlin, 1983), p120.

Acknowledgements

I thank my research director, Dave Shirley, for his support and considerable intellectual contributions to my work and Prof. E. F. Greene of Brown University for his major role in my undergraduate studies.

The experiments were performed in collaboration with two major research groups. Mike Knotek and Guillermo Loubriel from the Sandia National Laboratories made this thesis possible with their work, encouragement, advice, and generosity; I also thank Rick Stulen and Steve Haney for their help. It was also a pleasure to work with Richard Rosenberg and Vic Rehn from the Michelson Laboratory at China Lake, along with Phil LaRoe, Vern Jones, Al Green, and Peter Love.

The members of the Shirley group were close friends and colleagues during the past five years. Steve Kevan, Dave Denley, Danny Rosenblatt, Rich Davis, Gary Mason, and Geoff Thornton taught me about surface science in the beginning of my graduate career. John Barton, Charlie Bahr, and Prof. Zahid Hussain refined many of my notions about PSD before they were sent to the Physical Review. Dennis Trevor, John Barton, and Charlie Bahr invented the RPN data analysis program which spawned this thesis. I have also learned from Jim Pollard, Carlton Truesdale, Paul Kobrin, Dennis Trevor, Steve Southworth, Dennis Lindle, Lennie Klebanoff, Steve Robey, Phil Heimann, Hans Kerkhoff, Janice Reutt, Trish Ferrett, Albert Baca, and more recently, Alexis Schach von Wittenau and Margaret Schulz.

Wini Heppler and Barbara Moriguchi have been helpful in many ways. I thank Robert Mayer, Harry Morales, and John Yang on the staff at the Stanford Synchrotron Radiation Laboratory for going far beyond the call of duty.

I would like to acknowledge my friends in Berkeley, including Russ and Tom Blackadar, Bill Gary, Mike and Vicki Mayberry, Chris and Mary Freiberger, and Amelia Seyssel. I am grateful to my family for their love and support for the past twenty-seven years and I dedicate this thesis to my parents.

This report was done with support from the Department of Energy. Any conclusions or opinions expressed in this report represent solely those of the author(s) and not necessarily those of The Regents of the University of California, the Lawrence Berkeley Laboratory or the Department of Energy.

Reference to a company or product name does not imply approval or recommendation of the product by the University of California or the U.S. Department of Energy to the exclusion of others that may be suitable.